SIAM J. IMAGING SCIENCES
Vol. 7, No. 1, pp. 212–238

Optimal Transport with Proximal Splitting[*]

Nicolas Papadakis[†], Gabriel Peyré[‡], and Edouard Oudet[§]

Abstract. This article reviews the use of first order convex optimization schemes to solve the discretized dynamic optimal transport problem, initially proposed by Benamou and Brenier. We develop a staggered grid discretization that is well adapted to the computation of the L^2 optimal transport geodesic between distributions defined on a uniform spatial grid. We show how proximal splitting schemes can be used to solve the resulting large scale convex optimization problem. A specific instantiation of this method on a centered grid corresponds to the initial algorithm developed by Benamou and Brenier. We also show how more general cost functions can be taken into account and how to extend the method to perform optimal transport on a Riemannian manifold.

Key words. optimal transport, proximal splitting, convex optimization, image warping

AMS subject classifications. 90C25, 68U10

DOI. 10.1137/130920058

1. Introduction.

Optimal transport is a well-developed mathematical theory that defines a family of metrics between probability distributions [76]. These metrics measure the amplitude of an optimal displacement according to a so-called ground cost defined on the space supporting the distributions. The resulting distance is sometimes referred to as the Wasserstein distance in the case of L^p ground costs. The geometric nature of optimal transportation, as well as the ability to compute optimal displacements between densities, make this theory progressively mainstream in several applicative fields (see below). However, the numerical resolution of the optimal transportation problem raises several challenges. This article is focused on the computation of geodesics for the optimal transport metric associated with the L^2 cost. It reviews and extends the approach pioneered by Benamou and Brenier [8] from the perspective of proximal operator splitting in convex optimization. This shows the simplicity and efficiency of this method, which can easily be extended beyond the setting of optimal transport by considering various convex cost functions.

1.1. Previous works.

Applications of optimal transport. Early successes of applications of optimal transport were mostly theoretical, such as the derivation of functional inequalities [27] or the construction

[*] Received by the editors May 7, 2013; accepted for publication (in revised form) October 11, 2013; published electronically January 28, 2014. This work was partially funded by the French Agence Nationale de la Recherche (ANR, Project TOMMI) under reference ANR-11-BS01-014-01.

http://www.siam.org/journals/siims/7-1/92005.html

[†] IMB, Université Bordeaux 1, F-33405 Talence, France (nicolas.papadakis@math.u-bordeaux1.fr). This author's work was partially supported by the LEFE program of INSU (CNRS).

[‡] CEREMADE, Université Paris-Dauphine, 75775 Paris Cedex 16, France (gabriel.peyre@ceremade.dauphine.fr). This author's work was partially supported by the European Research Council (ERC project SIGMA-Vision).

[§] LJK, Université de Grenoble, Campus de Saint Martin d'Hères, BP 53, 38041 Grenoble Cedex 09, France (Edouard.Oudet@imag.fr).

of solutions of some nonlinear PDEs [52]. But recently, computational optimal transport has gained much interest and is progressively becoming mainstream in several applicative fields. In computer vision, the Wasserstein distance has been shown to outperform other metrics between distributions for machine learning tasks [69, 65]. In image processing, the warping provided by the optimal transport has been used for video restoration [31], color transfer [64], texture synthesis [39], and medical imaging registration [49]. It has also been applied to interpolation in computer graphics [13] and surface reconstruction in computational geometry [34]. Optimal transport is also used to model various physical phenomena, for instance in astrophysics [42] and oceanography [5].

Discrete optimal transport. The easiest way to discretize and compute numerically optimal transports is to consider finite sums of weighted Diracs. In this specific case, the optimal transport is a multivalued map between the Diracs' locations. Specific linear solvers can be used in this context, and in particular network and transportation simplices [28] can scale up to a few thousands of Dirac masses. Dedicated combinatorial optimization methods have been proposed, such as the auction algorithm [11], which can handle integer costs between the Diracs. In the even more restricted case of two distributions with the same number of Diracs with equal weights, the transportation is a bijection between the points and thus corresponds to the optimal assignment problem [19]. Combinatorial optimization methods such as the Hungarian algorithm [47] have roughly cubic complexity in the number of Diracs. Faster schemes exist for specific cost functions, such as the convex cost of the distance on the line (where it boils down to a sorting of the positions) and the circle [32], concave costs on the line [33], and the ℓ^1 distance [55]. The computation can be accelerated using multiscale clustering [59]. Note also that various approximations of the transportation distance have been proposed; see, for instance, [71].

Despite being numerically intensive for finely discretized distributions, this discrete transport framework has found many applications, such as for color transfer between images [67], shape retrieval [69], surface reconstruction [29], and interpolation for computer graphics [13].

Optimal transport and PDEs. The optimal transport for the L^2 ground cost has a special structure. It can be shown to be uniquely defined and to be the gradient of a convex function [16]. This implies that it is also the solution of the fully nonlinear Monge–Ampère PDE. Several methods have been proposed to discretize and solve this PDE, such as the method of [63], which converges to the Aleksandrov solution, and the one of [62], which converges to the viscosity solution of the equation. Alternative methods such as [30] and [38] are efficient for regular densities. A major difficulty in these approaches is dealing with compactly supported densities, which requires a careful handing of the boundary conditions. [43] proposes to enforce these conditions by iteratively solving a Monge–Ampere equation with Neumann boundary conditions. [10] introduces a method requiring the solution of a well-posed Hamilton–Jacobi equation. Another line of methods iteratively constructs mass-preserving mappings converging to the optimal transport [3]. This explicitly constructs the so-called polar factorization of the initial map; see also [6] for a different approach. This method is enhanced in [48] to avoid drifting from the preservation constraint during the iterations. These PDE-based approaches to the resolution of the optimal transport have found several applications, such as image registration [49], density regularization [18], optical flow [23], and grid generation [74].

Another line of research consists of using gradient flows where the gradient direction is computed according to the Wasserstein distance. This was initially proposed in [52] to build solutions to certain nonlinear PDEs. This technique is now being used to design numerical approximation schemes for the solution of these equations; see, for instance, [21, 36, 40].

Dynamical optimal transport. Instead of directly computing the transport, it is possible to consider the geodesic path between the two densities according to the Wasserstein metric (the so-called displacement interpolation [58]). For the L^2 ground cost, this geodesic is obtained by linear interpolation between the identity and the transport. The geodesic can thus be computed by first obtaining the transport and then evolving the densities. If one considers discrete sums of Diracs, this corresponds to solving a convex linear program and can also be understood as a Lagrangian approximation of the transport between (possibly continuous) densities that have been discretized. This approach is refined in [51], which considers discretization with a mixture of Gaussians.

It is also possible to consider an Eulerian formulation of the geodesic problem, for which densities along the path are discretized on a fixed spatial grid. Conservation of mass is achieved by introducing an incompressible velocity field transporting the densities. The breakthrough paper [8] shows that it is possible to perform a change of variables to obtain a convex problem. They propose numerically solving the discretized problem with a first order iterative method. We give further details below on this method in the section on proximal methods.

Geodesics between pairs of distributions can be extended to barycenters between an arbitrary finite collection of distributions. Existence and uniqueness of this barycenter is studied in [1]. Computing the barycenter between discrete distributions requires the resolution of a convex linear program that corresponds to a multimarginal optimal transportation, as proved in [1]. However, in sharp contrast with the case of two distributions, the special case of unweighted sums of Diracs is no longer equivalent to an assignment problem, which is known to be NP-hard [19]. Numerically computing this barycenter for large scale problems can, however, be tackled using a nonconvex formulation to solve for a Lagrangian discretization, which finds applications in image processing [68].

Generalized transport problems. The formulation of the geodesic computation as a convex optimization problem initiated by [8] enables the definition of various metrics obtained by changing the objective function. A penalization of the matching constraint [7] allows one to compute an unbalanced transport, where densities are not normalized to have the same mass. An interpolation between the L^2-Wasserstein and L^2 distances is proposed in [9]. Lastly, an interpolation between L^2-Wasserstein and H^{-1} distances is described in [35]. This extension relies in a crucial manner on the convexity of the extended objective function, which enables a theoretical analysis to characterize minimizing geodesics [20]. Convexity also allows one to use the numerical scheme that we propose with only slight modifications with respect to the L^2-Wasserstein case, as we detail in section 5.

Optimal transport on Riemannian manifolds. Many properties of the L^2-Wasserstein distance extend to the setting where the ground cost is the square of the geodesic distance on a Riemannian manifold. This includes in particular the existence and uniqueness of the transport map, which is the manifold exponential of the gradient of a semiconvex map [57]. Displacement interpolation for transport on manifolds has the same variational characterization as that introduced in [9] for Euclidean transport; see [77] for a detailed review of optimal transport on manifolds. Interpolation between pairs of measures generalizes to barycenters of a family of measures; see [53].

Displacement interpolation between two measures, each one composed of a single Dirac, amounts to computing a single geodesic curve on the manifold. Discretization and numerical solutions to this problem are numerous. A popular method is the fast marching algorithm introduced jointly by [70, 75] for isotropic Riemannian metrics (i.e., when the metric at each point is a scalar multiple of the identity) discretized on a rectangular grid. The complexity of the method is $O(N \log(N))$ operations, where N is the number of grid points. This algorithm has been extended to compute geodesics on two-dimensional (2-D) triangular meshes with only acute angles [54]. More general discretizations and the extension to Finsler metrics require the use of slower iterative schemes; see, for instance, [14].

Numerical computation of optimal transport on manifolds has been less studied. For weighted sums of Diracs, displacement interpolation is achieved by solving the linear program to compute the coupling between the Diracs and then advancing the Diracs with the corresponding weights and constant velocity along the geodesics. In this article, we propose extending the Eulerian discretization method [9] to solve for the displacement interpolation on a Riemannian manifold.

First order and proximal methods. The convex problem considered by Benamou and Brenier [8] can be recast as the optimization of a linear functional under second order conic constraints (see section 3.6 for more details). This class of programs can be solved in time polynomial with the desired accuracy using interior point methods; see, for instance, [61].

However, the special structure of the problem, especially when discretized on a uniform grid, makes it suitable for first order schemes and particularly proximal splitting methods. While these proximal methods do not reach the same convergence speed for arbitrary conic programs, they work well in practice for large scale problems, in particular when high accuracy is not mandatory, which is a common setup for problems in image processing. Proximal splitting schemes are first order optimization methods that allow one to minimize a sum of so-called simple functionals, possibly (for some methods) precomposed by linear operators. A functional is called "simple" when it is possible to compute its proximal operator (see expression (4.1) for its precise definition) either in closed form or with high accuracy using a few iterations of some subroutine. In this article, we focus our attention on the Douglas–Rachford algorithm, introduced by [56], and on primal-dual methods. We make use of the recently proposed method of [22], but other schemes could be used as well; see, for instance, [17]. We refer the reader to [25] and the references therein for more information about the properties of proximal maps and the associated proximal splitting schemes.

Note that the ALG2 algorithm proposed by [8] corresponds to applying the alternating direction method of multipliers (ADDM) [41] to the Fenchel–Rockafeller dual of the (primal) dynamical transport problem. As shown by [44, 37], this corresponds exactly to directly applying (a specific instantiation of) the Douglas–Rachford method to the primal problem; see section 4.6 for more details.

Fluid mechanics discretization. While Lagrangian methods utilize a mesh-free discretization (see, for instance, [51]), which typically tracks the movement of centers of mass during the transportation, Eulerian methods require a fixed discretization of the spatial domain. The most straightforward strategy is to use a uniform centered discretization of an axis-aligned domain, which is used in most previously cited works; see, for instance, [8, 3]. Because of the close connection between dynamical optimal transport and fluid dynamics, we advocate in this article the use of staggered grids [2], which better cope with the incompressibility condition.

1.2. Contributions. Our first contribution is to show how the method initially proposed in [8] is a specific instance of the Douglas–Rachford algorithm. This allows one to use several variations on the initial method, by changing the values of the two relaxation parameters and using different proximal splittings of the functional (possibly introducing auxiliary variables). Our second contribution is the introduction of a staggered grid discretization which is an efficient and convenient way to enforce incompressibility constraints. We show how this discretization fits into our proximal splitting methodology by introducing an interpolation operator and making use of either auxiliary variables or primal-dual methods. Our last contribution includes an exploration of several variations on the original convex transportation objective, the one proposed in [35] and a spatially varying penalization which can be interpreted as replacing the L^2 ground cost by a geodesic distance on a Riemannian manifold. Note that the MATLAB source code for reproducing the figures of this article is available online.[1]

2. Dynamical optimal transport formulation.

2.1. Optimal transport. In the following, we restrict our exposition to smooth maps $T : [0,1]^d \mapsto [0,1]^d$, where $d > 0$ is the dimension of the problem. A valid transport map T is a map that pushes forward the measure $f^0(x)\mathrm{d}x$ onto $f^1(x)\mathrm{d}x$. In term of densities, this corresponds to the constraint

$$f^0(x) = f^1(T(x))|\det(\partial T(x))|,$$

where $\partial T(x) \in \mathbb{R}^{d\times d}$ is the differential of T at x. This is known as the gradient equation. We call $\mathcal{T}(f^0, f^1)$ the set of transport that satisfies this constraint. An optimal transport T solves

$$\min_{T\in\mathcal{T}(f^0,f^1)} \int C(x, T(x))\mathrm{d}x, \tag{2.1}$$

where $C(x, y) \geqslant 0$ is the cost of assigning $x \in [0,1]^d$ to $y \in [0,1]^d$. In the case $C(x, y) = \|x - y\|^2$, the optimal value of (2.1), the so-called optimal transport distance, is often called the L^2-Wasserstein distance between the densities f^0 and f^1.

2.2. Fluid mechanics formulation. The geodesic path between the measures with densities $f^0(x)$ and $f^1(x)$ can be shown to have density $t \mapsto f(x, t)$, where $t \in [0,1]$ parameterizes the path, where

$$f(x,t) = f^0(T_t(x))|\det(\partial T_t(x))|, \quad \text{where} \quad T_t = (1-t)\mathrm{Id}_d + tT.$$

Benamou and Brenier showed in [8] that this geodesic solves the following nonconvex problem over the densities $f(x, t) \in \mathbb{R}$ and a velocity field $v(x, t) \in \mathbb{R}^2$:

$$\min_{(v,f)\in\mathcal{C}^0} \frac{1}{2}\int_{[0,1]^d}\int_0^1 f(x,t)\|v(x,t)\|^2\mathrm{d}t\mathrm{d}x, \tag{2.2}$$

[1] https://github.com/gpeyre/2013-SIIMS-ot-splitting/

under the set of nonlinear constraints

$$\mathcal{C}^0 = \left\{(v,f)\ ;\ \partial_t f + \mathrm{div}_x(fv) = 0,\ v(0,\cdot) = v(1,\cdot) = 0,\ f(\cdot,0) = f^0,\ f(\cdot,1) = f^1\right\}, \tag{2.3}$$

where the first relation in $\mathcal{C}^0$ is the continuity equation. We impose homogeneous Neumann conditions on the velocity field v which are the more natural boundary conditions in the case of the square. Notice that both Neumann and Dirichlet boundary conditions can easily be implemented in our framework. The difference relies in the projection step on the divergence constraint. This step, which is carried out using the fast Fourier transform algorithm, has to be adapted depending on the chosen boundary conditions. We refer to [43, 10] for relevant boundary conditions for other convex geometries. The temporal boundary constraints on f impose a match with the input density data.

From a theoretical point of view, the natural setting for proving existence of minimizers of (2.2) is to relax the variational problem and perform the optimization over the Banach space of Radon measures (i.e., finite Borel measures). This space of Radon measures is a subspace of the space of distributions, and the incompressibility constraint (2.3) should be understood in the sense of distributions. We refer the interested reader to [20] for more details regarding the theoretical analysis of a class of variational problems generalizing (2.2).

Note that once an optimal vector field v solving (2.2) has been computed, it is possible to recover an optimal transport T by integrating the flow in time. From a given $x \in [0,1]^d$, we define the solution $t \mapsto T_t(x)$ solving

$$T_0(x) = x \quad \text{and} \quad \forall\, t > 0, \quad \frac{\partial T_t(x)}{\partial t} = v(T_t(x), t).$$

The optimal transport is then obtained at $t = 1$, i.e., $T = T_1$; see [8] for more details.

Following [8], introducing the change of variable $(v, f) \mapsto (m, f)$, where m is the momentum $m = fv$, one obtains a convex optimization problem over the pair (f, m):

$$\min_{(m,f)\in\mathcal{C}} \mathcal{J}(m,f) = \int_{[0,1]^d}\int_0^1 J(m(x,t), f(x,t))\mathrm{d}t\mathrm{d}x, \tag{2.4}$$

$$\text{where} \quad \forall\,(m,f) \in \mathbb{R}^d \times \mathbb{R}, \quad J(m,f) = \begin{cases} \frac{\|m\|^2}{2f} & \text{if } f > 0,\\ 0 & \text{if } (m,f) = (0,0),\\ +\infty & \text{otherwise,}\end{cases} \tag{2.5}$$

and the set of linear constraints reads

$$\mathcal{C} = \left\{(m,f)\ ;\ \partial_t f + \mathrm{div}_x(m) = 0,\ m(0,\cdot) = m(1,\cdot) = 0,\ f(\cdot,0) = f^0,\ f(\cdot,1) = f^1\right\}.$$

3. Discretized dynamic optimal transport.

For simplicity of exposure, we describe the discretization for the 1-D case. It extends verbatim to higher-dimensional discretization $d > 1$.

3.1. Centered grid.

We denote by $N + 1$ the number of discretization points in space, and by $P + 1$ the number of discretization points in time. We introduce the centered grid discretizing the space-time square $[0,1]^2$ in $(N+1) \times (P+1)$ points as

$$\mathcal{G}_{\mathrm{c}} = \left\{(x_i = i/N,\ t_j = j/P) \in [0,1]^2\ ;\ 0 \leqslant i \leqslant N, 0 \leqslant j \leqslant P\right\}.$$

We denote by

$$V = (m, f) \in \mathcal{E}_{\mathrm{c}} = (m_{i,j}, f_{i,j})_{0 \leqslant i \leqslant N}^{0 \leqslant j \leqslant P}$$

the variables discretized on the centered grid, where $\mathcal{E}_{\mathrm{c}} = (\mathbb{R}^{d+1})^{\mathcal{G}_{\mathrm{c}}} = (\mathbb{R}^2)^{\mathcal{G}_{\mathrm{c}}}$ is the finite-dimensional space of centered variables.

3.2. Staggered grid. The use of a staggered grid is very natural in the context of the discretization of a divergence operator associated with a vector field $u = (u_i)_{i=1}^d$ on $\mathbb{R}^d$. (We focus on the case $d = 2$ here.) The basic idea is to allow an accurate evaluation of every partial derivative $\partial_{x_i} u_i(P)$ at prescribed nodes P of a Cartesian grid using standard centered finite differences. One way to perform this computation is to impose to the grid on which the u_i scalar field is defined to be centered on P points along the x_i direction. This simple requirement forces the u_i scalar field to be defined on different grids. The resulting discrete vector field gives us the possibility of evaluating the divergence operator by a uniform standard centered scheme, which is not possible using a single grid of discretization for every component of $(u_i)_i$. As a consequence, similarly to the discretization of PDEs in incompressible fluid dynamics (see, for instance, [50]), we consider a staggered grid discretization, which is more relevant for dealing with the continuity equation and is defined as

$$\mathcal{G}_{\mathrm{s}}^x = \left\{ \left(x_i = \frac{i+1/2}{N},\, t_j = \frac{j}{P} \right) \in \frac{[-1, 2N+1]}{2N} \times [0,1]\, ; -1 \leqslant i \leqslant N, 0 \leqslant j \leqslant P \right\},$$
$$\mathcal{G}_{\mathrm{s}}^t = \left\{ \left(x_i = \frac{i}{N},\, t_j = \frac{j+1/2}{P} \right) \in [0,1] \times \frac{[-1, 2P+1]}{2P}\, ;\ 0 \leqslant i \leqslant N, -1 \leqslant j \leqslant P \right\}.$$

From these definitions, we see that $\mathcal{G}_{\mathrm{s}}^x$ contains $(N+2) \times (P+1)$ points, and $\mathcal{G}_{\mathrm{s}}^t$ corresponds to an $(N+1) \times (P+2)$ discretization. We finally denote by

$$U = (\bar{m}, \bar{f}) \in \mathcal{E}_{\mathrm{s}} = ((\bar{m}_{i,j})_{-1 \leqslant i \leqslant N}^{0 \leqslant j \leqslant P}, (\bar{f}_{i,j})_{0 \leqslant i \leqslant N}^{-1 \leqslant j \leqslant P})$$

the variables discretized on the staggered grid, where $\mathcal{E}_{\mathrm{s}} = \mathbb{R}^{\mathcal{G}_{\mathrm{s}}^x} \times \mathbb{R}^{\mathcal{G}_{\mathrm{s}}^t}$ is the finite-dimensional space of staggered variables.

3.3. Interpolation and divergence operators. We introduce a midpoint interpolation operator $\mathcal{I} : \mathcal{E}_{\mathrm{s}} \to \mathcal{E}_{\mathrm{c}}$, where, for $U = (\bar{m}, \bar{f}) \in \mathcal{E}_{\mathrm{s}}$, we define $\mathcal{I}(U) = (m, f) \in \mathcal{E}_{\mathrm{c}}$ as

$$\forall\, 0 \leqslant i \leqslant N, \quad \forall\, 0 \leqslant j \leqslant P, \quad \left\{ \begin{array}{ll} m_{i,j} &= (\bar{m}_{i-1,j} + \bar{m}_{i,j})/2, \\ f_{i,j} &= (\bar{f}_{i,j-1} + \bar{f}_{i,j})/2. \end{array} \right. \tag{3.1}$$

The space-time divergence operator $\mathrm{div} : \mathcal{E}_{\mathrm{s}} \to \mathbb{R}^{\mathcal{G}_{\mathrm{c}}}$ is defined, for $U = (\bar{m}, \bar{f}) \in \mathcal{E}_{\mathrm{s}}$, as

$$\forall\, 0 \leqslant i \leqslant N,\ \forall\, 0 \leqslant j \leqslant P, \quad \mathrm{div}(U)_{i,j} = N(\bar{m}_{i,j} - \bar{m}_{i-1,j}) + P(\bar{f}_{i,j} - \bar{f}_{i,j-1}).$$

3.4. Boundary constraints. We extract the boundary values on the staggered grid using the linear operator b, defined for $U = (\bar{m}, \bar{f}) \in \mathcal{E}_{\mathrm{s}}$ as

$$b(U) = \left((\bar{m}_{-1,j}, \bar{m}_{N,j})_{j=0}^P, (\bar{f}_{i,-1}, \bar{f}_{i,P})_{i=0}^N \right) \in \mathbb{R}^{P+1} \times \mathbb{R}^{P+1} \times \mathbb{R}^{N+1} \times \mathbb{R}^{N+1}.$$

We impose the following boundary values:

$$b(U) = b_0, \quad \text{where} \quad b_0 = (0, 0, f^0, f^1) \in \mathbb{R}^{P+1} \times \mathbb{R}^{P+1} \times \mathbb{R}^{N+1} \times \mathbb{R}^{N+1},$$

where $f^0, f^1 \in \mathbb{R}^{N+1}$ are the discretized initial (time $t = 0$) and final (time $t = 1$) densities and the spatial boundary constraint $0 \in \mathbb{R}^P$ on the momentum $m = fv$ comes from the discretized Neumann boundary conditions on the velocity field v. Notice that in the 2-D or 3-D cases, Neumann and Dirichlet boundary conditions do not coincide. For instance in two dimensions, Neumann conditions are equivalent to forcing the first component of $\bar{m}$ to be zero only on the vertical segments of the boundary, whereas the second component vanishes only on the horizontal ones.

3.5. Discrete convex problem.

The initial continuous problem (2.4) is approximated on the discretization grid by solving the finite-dimensional convex problem

$$\min_{U \in \mathcal{E}_\mathrm{s}} \mathcal{J}(\mathcal{I}(U)) + \iota_\mathcal{C}(U). \tag{3.2}$$

Here, for a closed convex set $\mathcal{C}$, we have denoted its associated indicator function by

$$\iota_\mathcal{C}(U) = \begin{cases} 0 & \text{if } U \in \mathcal{C}, \\ +\infty & \text{otherwise.} \end{cases}$$

The discrete objective functional $\mathcal{J}$ reads for $V = (m, f) \in \mathcal{E}_\mathrm{c}$

$$\mathcal{J}(V) = \sum_{k \in \mathcal{G}_\mathrm{c}} J(m_k, f_k), \tag{3.3}$$

where we denote by $k = (i, j) \in \mathcal{G}_\mathrm{c}$ the indexes on the centered grid, and the functional J is defined in (2.5).

The constraint set $\mathcal{C}$ corresponds to the divergence-free constraint together with the boundary constraints

$$\mathcal{C} = \{U \in \mathcal{G}_\mathrm{s} \; ; \; \mathrm{div}(U) = 0 \quad \text{and} \quad b(U) = b_0\}.$$

3.6. Second order cone programming formulation.

The discretized problem (3.2) can be equivalently solved as the following minimization over variables $(U, V, W) \in \mathcal{E}_\mathrm{s} \times \mathcal{E}_\mathrm{c} \times \mathbb{R}^{\mathcal{G}_\mathrm{c}}$:

$$\min_{(V,W) \in \mathcal{K}, V = \mathcal{I}(U)} \sum_{k \in \mathcal{G}_\mathrm{c}} W_k, \tag{3.4}$$

where $\mathcal{K}$ is the product of (rotated) Lorentz cones,

$$\mathcal{K} = \left\{(V = (\bar{m}, \bar{f}), W) \in \mathcal{E}_\mathrm{c} \times \mathbb{R}^{\mathcal{G}_\mathrm{c}} \; ; \; \forall\, k \in \mathcal{G}_\mathrm{c}, \; \|\bar{m}_k\|^2 - W_k \bar{f}_k \leqslant 0\right\}.$$

Problem (3.4) is a specific instance of a so-called second order cone program (SOCP), which can be solved in time polynomial with the accuracy using interior point methods (see section 1.1 for more details). As already mentioned in section 1.1, we focus in this article on proximal splitting methods, which are more adapted to large scale imaging problems.

4. Proximal splitting algorithms.

In this section, we review some splitting schemes and detail how they can be applied to solving (3.2). This requires computing the proximal operators of the cost function J and of the indicator of the constraint set $\mathcal{C}$.

4.1. Proximal operators and splitting schemes.

The minimization of a convex functional F over some Hilbert space $\mathcal{H}$ requires the use of algorithms that are tailored to the specific properties of the functional. Smooth functions can be minimized through the use of gradient descent steps, which amounts to repeatedly applying the mapping $\mathrm{Id}_{\mathcal{H}} - \gamma\nabla F$ for a small enough step size $\gamma > 0$. Such schemes cannot be used for nonsmooth functions such as the one considered in (3.2).

A popular class of first order methods, so-called proximal splitting schemes, replaces the gradient descent step by the application of the proximal operator. The proximal operator $\mathrm{Prox}_{\gamma F} : \mathcal{H} \to \mathcal{H}$ of a convex, lower semicontinuous, and proper functional $F : \mathcal{H} \to \mathbb{R}\cup\{+\infty\}$ is defined as

$$\mathrm{Prox}_{\gamma F}(z) = \underset{\tilde{z}\in\mathcal{H}}{\mathrm{argmin}}\ \frac{1}{2}\|z - \tilde{z}\|^2 + \gamma F(\tilde{z}). \tag{4.1}$$

This proximal operator is a single-valued map, which is related to the set-valued map of the subdifferential ∂F by the relationship $\mathrm{Prox}_{\gamma F} = (\mathrm{Id}_{\mathcal{H}} + \gamma\partial F)^{-1}$. This is why the application of $\mathrm{Prox}_{\gamma F}$ is often referred to as an implicit descent step, which should be compared with the explicit gradient descent step, $\mathrm{Id}_{\mathcal{H}} - \gamma\nabla F$.

Proximal operators enjoy several interesting algebraic properties which help the practitioner to compute them for complicated functionals. A typical example is the computation of the proximal operator of the Legendre–Fenchel transform of a function. The Legendre–Fenchel transform of F is defined as

$$F^*(w) = \max_{z\in\mathcal{H}}\ \langle z,\, w\rangle - F(z). \tag{4.2}$$

Note that, thanks to Moreau's identity [60],

$$\forall\, w \in \mathcal{H}, \quad \mathrm{Prox}_{\gamma F^\star}(w) = w - \gamma\, \mathrm{Prox}_{F/\gamma}(w/\gamma), \tag{4.3}$$

computing the proximal operator of F^* has the same complexity as computing the proximal operator of F.

To enable the use of these proximal operators within an optimization scheme, it is necessary to be able to compute them efficiently. We call a function F such that $\mathrm{Prox}_{\gamma F}$ can be computed in closed form a *simple function*. It is often the case that the function to be minimized is not simple. The main idea underlying proximal splitting methods is to decompose this function into a sum of simple functions (possibly composed of linear operators). We detail below three popular splitting schemes, the Douglas–Rachford (DR) algorithm, the alternating direction method of multipliers (ADMM), and a primal-dual (PD) algorithm. We refer the reader to [25] for a detailed review of proximal operators and proximal splitting schemes.

4.2. Computing $\mathrm{Prox}_{\gamma\mathcal{J}}$.

The following proposition shows that the functional $\mathcal{J}$ defined in (3.3) is simple, in the sense that its proximal operator can be computed in closed form.

Proposition 1. *One has*

$$\forall\, V \in \mathcal{E}_c, \quad \mathrm{Prox}_{\gamma\mathcal{J}}(V) = (\mathrm{Prox}_{\gamma J}(V_k))_{k\in\mathcal{G}_c},$$

where, for all $(\tilde{m}, \tilde{f}) \in \mathbb{R}^d \times \mathbb{R}$*,*

$$\operatorname{Prox}_{\gamma J}(\tilde{m}, \tilde{f}) = \begin{cases} (\mu(f^\star), f^\star) & \text{if } f^\star > 0, \\ (0,0) & \text{otherwise,} \end{cases}$$

$$\text{where} \quad \forall\, f \geqslant 0, \quad \mu(f) = \frac{f\tilde{m}}{f+\gamma}, \tag{4.4}$$

and $f^\star$ *is the largest real root of the third order polynomial equation in* X*:*

$$P(X) = (X - \tilde{f})(X+\gamma)^2 - \frac{\gamma}{2}\|\tilde{m}\|^2 = 0. \tag{4.5}$$

Proof. We define $(m, f) = \operatorname{Prox}_{\gamma J}(\tilde{m}, \tilde{f})$. If $f > 0$, since J is C^1 and is strongly convex on $\mathbb{R}^d \times \mathbb{R}^{+,*}$, necessarily (m, f) is the unique solution of $\nabla J(m, f) = 0$, which reads

$$\begin{cases} \gamma \frac{m}{f} + m - \tilde{m} = 0, \\ -\gamma \frac{\|m\|^2}{f^2} + f - \tilde{f} = 0. \end{cases}$$

Reformulating these equations leads to the following equivalent conditions:

$$P(f) = 0 \quad \text{and} \quad m = \mu(f).$$

This shows that if P has at least one strictly positive real root $f^\star$, it is necessarily unique and that $(f = f^\star, m = \mu(f^\star))$. On the contrary, one necessarily has $f = 0$ and, by definition of J, $m = 0$ as well. ■

4.3. Computing $\operatorname{Proj}_{\mathcal{C}}$.

The proximal mapping of $\iota_{\mathcal{C}}$ is $\operatorname{Proj}_{\mathcal{C}}$, the orthogonal projector on the convex set $\mathcal{C}$. This is an affine set that can be written as

$$\mathcal{C} = \{U = (m, f) \in \mathcal{E}_{\mathrm{s}} \; ; \; AU = y\}, \quad \text{where } AU = (\operatorname{div}(U), b(U)) \quad \text{and} \quad y = (0, b_0).$$

This projection can be computed by solving a linear system as

$$\operatorname{Proj}_{\mathcal{C}} = (\mathrm{Id} - A^*\Delta^{-1}A) + A^*\Delta^{-1}y,$$

where applying $\Delta^{-1} = (AA^*)^{-1}$ requires solving a Poisson equation on the centered grid $\mathcal{G}_{\mathrm{c}}$ with the prescribed boundary conditions. This can be achieved with a fast Fourier transform in $O(NP\log(NP))$ operations, where N and P are the numbers of spatial and temporal points; see [73].

4.4. The DR solver.

DR algorithm. The DR algorithm [56] is a proximal splitting method that allows one to solve

$$\min_{z \in \mathcal{H}} G_1(z) + G_2(z), \tag{4.6}$$

where G_1 and G_2 are two simple functions defined on some Hilbert space $\mathcal{H}$.

The iterations of the DR algorithm define a sequence $(z^{(\ell)}, w^{(\ell)}) \in \mathcal{H}^2$ using an initial $(z^{(0)}, w^{(0)}) \in \mathcal{H}^2$ and

$$\begin{aligned} w^{(\ell+1)} &= w^{(\ell)} + \alpha(\operatorname{Prox}_{\gamma G_1}(2z^{(\ell)} - w^{(\ell)}) - z^{(\ell)}), \\ z^{(\ell+1)} &= \operatorname{Prox}_{\gamma G_2}(w^{(\ell+1)}). \end{aligned} \tag{4.7}$$

If $0 < \alpha < 2$ and $\gamma > 0$, one can show that $z^{(\ell)} \to z^\star$, which is a solution of (4.6); see [24] for more details.

In the following, we describe several possible ways to map the optimal transport optimization (3.2) into the splitting formulation (4.6), which in turn gives rise to four different algorithms.

Asymmetric-DR (A-DR) splitting scheme. We recast the initial optimal transport problem (3.2) as an optimization of the form (4.6) by using the variables

$$z = (U, V) \in \mathcal{H} = \mathcal{E}_{\mathrm{s}} \times \mathcal{E}_{\mathrm{c}}$$

and setting the functionals minimized as

$$\forall\, z = (U, V) \in \mathcal{E}_{\mathrm{s}} \times \mathcal{E}_{\mathrm{c}}, \quad G_1(z) = \mathcal{J}(V) + \iota_{\mathcal{C}}(U) \quad \text{and} \quad G_2(z) = \iota_{\mathcal{C}_{s,c}}(z).$$

In this expression, $\mathcal{C}_{s,c}$ is the constraint set that couples staggered and centered variables,

$$\mathcal{C}_{s,c} = \{z = (U, V) \in \mathcal{E}_{\mathrm{s}} \times \mathcal{E}_{\mathrm{c}} \; ; \; V = \mathcal{I}(U)\},$$

and $\mathcal{I}$ is the interpolation operator defined in (3.1).

Both G_1 and G_2 are simple functions since

$$\operatorname{Prox}_{\gamma G_1}(U, V) = (\operatorname{Proj}_{\mathcal{C}}(U), \operatorname{Prox}_{\gamma \mathcal{J}}(V)), \tag{4.8}$$

$$\operatorname{Prox}_{\gamma G_2}(U, V) = \operatorname{Proj}_{\mathcal{C}_{s,c}}(U, V) = (\tilde{U}, \mathcal{I}(\tilde{U})), \quad \text{where } \tilde{U} = (\mathrm{Id} + \mathcal{I}^*\mathcal{I})^{-1}(U + \mathcal{I}^*(V)), \tag{4.9}$$

where $\mathcal{I}^*$ is the adjoint of the linear interpolation operator. Note that computing $\operatorname{Proj}_{\mathcal{C}_{s,c}}$ requires solving a linear system, but this system is separable along each dimension of the discretization grid, so it requires only solving a series of small linear systems. Furthermore, since the corresponding inverse matrix is the same along each dimension, we explicitly precompute the inverse of these $d + 1$ matrices.

In our case, the iterates variables appearing in (4.7) read $z^{(\ell)} = (U^{(\ell)}, V^{(\ell)})$, which allows one to retrieve an approximation $f^{(\ell)}$ of the transport geodesic as $U^{(\ell)} = (m^{(\ell)}, f^{(\ell)})$.

A nice feature of this scheme A-DR is that the iterates always satisfy $U^{(\ell)} \in \mathcal{C}$, but in general one does not have $V^{(\ell)} = \mathcal{I}(U^{(\ell)})$.

Asymmetric-DR' (A-DR') splitting scheme. In the DR algorithm (4.7), the functionals G_1 and G_2 do not play a symmetric role. One thus obtains a different algorithm (that we denote as A-DR'), by simply exchanging the definitions of G_1 and G_2 in (4.8). Using this scheme A-DR', one has $V^{(\ell)} = \mathcal{I}U^{(\ell)}$, but in general $U^{(\ell)}$ is not in the constraint set $\mathcal{C}$.

Symmetric-DR (S-DR) splitting scheme. In order to restore symmetry between the functionals $\mathcal{J}$ and $\iota_{\mathcal{C}}$ involved in the minimization algorithm, one can consider the formulation

$$z = (U, V, \tilde{U}, \tilde{V}) \in \mathcal{H} = (\mathcal{E}_{\rm s} \times \mathcal{E}_{\rm c})^2$$

using the functionals

$$G_1(z) = \mathcal{J}(V) + \iota_{\mathcal{C}}(U) + \iota_{\mathcal{C}_{s,c}}(\tilde{U}, \tilde{V}) \quad \text{and} \quad G_2(z) = \iota_{\mathcal{D}}(z),$$

where $\mathcal{D}$ is the diagonal constraint

$$\mathcal{D} = \left\{ z = (U, V, \tilde{U}, \tilde{V}) \in \mathcal{H} \; ; \; U = \tilde{U} \quad \text{and} \quad V = \tilde{V} \right\}. \tag{4.10}$$

These functionals are simple since, for $z = (U, V, \tilde{U}, \tilde{V}) \in \mathcal{H}$, one has

$$\begin{aligned} \operatorname{Prox}_{\gamma G_1}(z) &= \left(\operatorname{Proj}_{\mathcal{C}}(U), \operatorname{Prox}_{\gamma \mathcal{J}}(V), \operatorname{Proj}_{\mathcal{C}_{s,c}}(\tilde{U}, \tilde{V}) \right) \\ \text{and} \quad \operatorname{Prox}_{\gamma G_2}(z) &= \frac{1}{2} \left(U + \tilde{U}, V + \tilde{V}, U + \tilde{U}, V + \tilde{V} \right). \end{aligned}$$

The splitting reformulation of the form (4.10) was introduced in [72], and the corresponding DR scheme, extended to a sum of an arbitrary number of functionals, is detailed in [66, 26].

Symmetric-DR' (S-DR') splitting scheme. Similarly to the relationship between the A-DR and A-DR' algorithms, it is possible to define an S-DR' algorithm by reversing the roles of G_1 and G_2 in the algorithm S-DR.

4.5. The PD solver.

PD algorithms such as the relaxed Arrow–Hurwicz method introduced in [22] allow one to minimize functionals of the form $G_1 + G_2 \circ A$, where A is a linear operator and G_1, G_2 are simple functions. One can thus directly apply this method to problem (3.2) with $G_2 = \mathcal{J}$, $A = \mathcal{I}$, and $G_1 = \iota_{\mathcal{C}}$.

The iterations compute a sequence $(U^{(\ell)}, \Upsilon^{(\ell)}, V^{(\ell)}) \in \mathcal{E}_{\rm s} \times \mathcal{E}_{\rm s} \times \mathcal{E}_{\rm c}$ of variables from an initial $(\Upsilon^{(0)}, V^{(0)})$ according to

$$\begin{aligned} V^{(\ell+1)} &= \operatorname{Prox}_{\sigma G_2^*}(V^{(\ell)} + \sigma \mathcal{I} \Upsilon^{(\ell)}), \\ U^{(\ell+1)} &= \operatorname{Prox}_{\tau G_1}(U^{(\ell)} - \tau \mathcal{I}^* V^{(\ell+1)}), \\ \Upsilon^{(\ell+1)} &= U^{(\ell+1)} + \theta(U^{(\ell+1)} - U^{(\ell)}). \end{aligned} \tag{4.11}$$

Note that $\operatorname{Prox}_{\sigma G_2^*}$ can be computed using $\operatorname{Prox}_{G_2}$ following (4.3). If $0 \leqslant \theta \leqslant 1$ and $\sigma\tau\|\mathcal{I}\|^2 < 1$, then one can prove that $U^{(\ell)} \to U^\star$, which is a solution of (3.2); see [22].

The case $\theta = 0$ corresponds to the Arrow–Hurwicz algorithm [4], and the general case can be interpreted as a preconditioned version of the ADDM algorithm, as detailed in [22].

4.6. ADMM solver on a centered grid.

In this section, we give some details about the relationship between the algorithm ALG2 developed by Benamou and Brenier in [8] and our DR algorithms. The original paper [8] considers a finite difference implementation on a centered grid, which leads to solving the following optimization problem:

$$\min_{V \in \mathcal{E}_{\rm c}} \mathcal{J}(V) + \iota_{\tilde{\mathcal{C}}}(V), \quad \text{where } \tilde{\mathcal{C}} = \{ V \in \mathcal{E}_{\rm s} \; ; \; AV = y \}, \tag{4.12}$$

where A is this time defined on a centered grid.

Primal problem. The minimization (4.12) has the form

$$\min_{z\in\mathcal{H}} F\circ A(z)+G(z), \tag{4.13}$$

where $A:\mathcal{H}\to\tilde{\mathcal{H}}$ is a linear operator and $F\circ A$ and G are supposed to be simple functions.

For the optimal transport (OT) problem on a centered grid (4.12), the identification is obtained by setting

$$F=\iota_{\{y\}} \quad\text{and}\quad G=\mathcal{J},$$

which are indeed simple functions. One can use the DR algorithm (4.7) with

$$G_1=F\circ A \quad\text{and}\quad G_2=G \tag{4.14}$$

to solve problems of the form (4.13). Of course, the variants A-DR', S-DR, and S-DR' considered in section 4.4 could be used as well on a centered grid. Since we focus on the relationship with the work [8], we consider only the splitting (4.14).

Dual problem. Following [8], one can consider the Fenchel–Rockafeller dual to the primal program (4.13), which reads

$$\max_{s\in\tilde{\mathcal{H}}} -\left(G^*\circ(-A^*)(s)+F^*(s)\right). \tag{4.15}$$

In the specific setting of the OT problem (4.12), $F^*(p)=\langle y,\,p\rangle$, and the following proposition, proved in [8], shows that $G^*=\mathcal{J}^*$ is a projector on a convex set (which is a consequence of the fact that $\mathcal{J}$ is a 1-homogenous functional).

Proposition 2. *One has*

$$\mathcal{J}^*=\iota_{\mathcal{C}_\mathcal{J}}, \quad \textit{where} \quad \begin{cases} \mathcal{C}_\mathcal{J}=\{V\in\mathcal{E}_c\,;\,\forall\,k\in\mathcal{G}_c,\ V_k\in\mathcal{C}_J\}\,,\\ \mathcal{C}_J=\left\{(a,b)\in\mathbb{R}^d\times\mathbb{R}\,;\,\|a\|^2+2b\leqslant 0\right\}. \end{cases}$$

Proof. The Legendre–Fenchel transform (4.2) of the functional J defined in (2.5) at point $(a,b)\in\mathbb{R}^d\times\mathbb{R}$ reads

$$J^*(a,b)=\max_{(m,f)\in\mathbb{R}^d\times\mathbb{R}}\langle a,\,m\rangle+\langle b,\,f\rangle-\frac{m^2}{2f},$$

where we just focus on the case $f>0$, since $f=0$ (resp., $f<0$) will always give $J^*=0$ (resp., $J^*=-\infty$). The optimality conditions are given by

$$a=\frac{m}{f}\quad\text{and}\quad b=-\frac{m^2}{2f^2}.$$

Hence, we have that

$$\begin{aligned} J^*(a,b)&=\max_{(m,f)\in\mathcal{E}_c} f\left(\left\langle a,\,\frac{m}{f}\right\rangle+b\right)-\frac{m^2}{2f^2}\\ &=\max_{(m,f)\in\mathcal{E}_c} f\left(\langle a,\,a\rangle+2b\right), \end{aligned}$$

which is 0 if $\|a\|^2+2b\leqslant 0$ and $+\infty$ otherwise. ■

Note that one can use the Moreau identity (4.3) to compute the proximal operator of J using the orthogonal projection on $\mathcal{C}_J$ and vice versa:

$$\mathrm{Prox}_{\gamma J}(v)=v-\gamma\,\mathrm{Proj}_{\mathcal{C}_J}(v/\gamma).$$

The ADMM. The ADMM is an algorithm for solving a minimization of the form

$$\min_{s\in\tilde{\mathcal{H}}} H\circ B(s)+K(s), \tag{4.16}$$

where we assume that the function $K^*\circ B^*$ is simple and that $B:\tilde{\mathcal{H}}\to\mathcal{H}$ is injective. It was initially proposed in [45, 46].

We introduce the Lagrangian associated with (4.16) to account for an auxiliary variable $q\in\mathcal{H}$ satisfying $q=Bs$ with a multiplier variable $v\in\mathcal{H}$,

$$\forall\,(s,q,v)\in\tilde{\mathcal{H}}\times\mathcal{H}\times\mathcal{H},\quad L(s,q,v)=K(s)+H(q)+\langle v,\,Bs-q\rangle,$$

and the augmented Lagrangian for $\gamma>0$,

$$\forall\,(s,q,v)\in\tilde{\mathcal{H}}\times\mathcal{H}\times\mathcal{H},\quad L_\gamma(s,q,v)=L(s,q,v)+\frac{\gamma}{2}\|Bs-q\|^2.$$

The ADMM algorithm generates iterates $(s^{(\ell)},q^{(\ell)},v^{(\ell)})\in\tilde{\mathcal{H}}\times\mathcal{H}\times\mathcal{H}$ as follow:

$$\begin{aligned} s^{(\ell+1)}&=\operatorname*{argmin}_s L_\gamma(s,q^{(\ell)},v^{(\ell)}),\\ q^{(\ell+1)}&=\operatorname*{argmin}_q L_\gamma(s^{(\ell+1)},q,v^{(\ell)}),\\ v^{(\ell+1)}&=v^{(\ell)}+\gamma(Bs^{(\ell+1)}-q^{(\ell+1)}). \end{aligned}\tag{4.17}$$

This scheme can be shown to converge for any $\gamma>0$; see [45, 46]. A recent review of the ADMM algorithm and its applications in machine learning can be found in [15].

We introduce the proximal operator $\mathrm{Prox}^B_{\gamma F}:\mathcal{H}\to\tilde{\mathcal{H}}$ with a metric induced by an injective linear map B:

$$\forall\,z\in\mathcal{H},\quad \mathrm{Prox}^B_{K/\gamma}(z)=\operatorname*{argmin}_{s\in\tilde{\mathcal{H}}}\frac{1}{2}\|Bs-z\|^2+\frac{1}{\gamma}K(s). \tag{4.18}$$

One can then rewrite the ADMM iterations (4.17) using proximal maps

$$\begin{aligned} s^{(\ell+1)}&=\mathrm{Prox}^B_{K/\gamma}(q^{(\ell)}-u^{(\ell)}),\\ q^{(\ell+1)}&=\mathrm{Prox}_{H/\gamma}(Bs^{(\ell+1)}+u^{(\ell)}),\\ u^{(\ell+1)}&=u^{(\ell)}+Bs^{(\ell+1)}-q^{(\ell+1)}, \end{aligned}\tag{4.19}$$

where we have performed the change of variables $u^{(\ell)}=v^{(\ell)}/\gamma$ to simplify the notation.

The following proposition shows that if $K^*\circ B^*$ is simple, one can indeed perform the ADMM algorithm. Note that in the case $\mathcal{H}=\tilde{\mathcal{H}}$ and $B=\mathrm{Id}_{\mathcal{H}}$, one recovers Moreau's identity (4.3).

Proposition 3. *One has*

$$\forall\,z\in\mathcal{H},\quad \mathrm{Prox}^B_{K/\gamma}(z)=B^+\left(z-\frac{1}{\gamma}\mathrm{Prox}_{\gamma K^*\circ B^*}(\gamma z)\right).$$

Proof. We denote by $\mathcal{U} = \partial K$ the set-valued maximal monotone operator. Then $\partial K^* = \mathcal{U}^{-1}$, where $\mathcal{U}^{-1}$ is the set-valued inverse operator, and $\partial(K^* \circ B^*) = B \circ \mathcal{V} \circ B^*$. One has $\mathrm{Prox}_{\gamma K^* \circ B^*} = (\mathrm{Id} + \gamma\mathcal{V})^{-1}$, which is a single-valued operator. Denoting $s = \mathrm{Prox}^B_{K/\gamma}(z)$, the optimality conditions of (4.18) lead to

$$0 \in B^*(Bs - z) + \frac{1}{\gamma}\mathcal{U}(s) \iff s \in \mathcal{U}^{-1}\left(\gamma B^* Bs - \gamma B^* z\right) \iff \gamma Bs \in \gamma\mathcal{V}\left(\gamma z - \gamma Bs\right) \tag{4.20}$$

$$\iff \gamma Bs \in (\mathrm{Id} + \gamma\mathcal{V})\left(\gamma z - \gamma Bs\right) + \gamma Bs - \gamma z \iff \gamma z \in (\mathrm{Id} + \gamma\mathcal{V})\left(\gamma z - \gamma Bs\right) \tag{4.21}$$

$$\iff \gamma z - \gamma Bs = (\mathrm{Id} + \gamma\mathcal{V})^{-1}(\gamma z) \iff s = B^+\left(z - \frac{1}{\gamma}(\mathrm{Id} + \gamma\mathcal{V})^{-1}(\gamma z)\right), \tag{4.22}$$

where we used the fact that B is injective. ■

Equivalence between ADMM and DR. The ALG2 algorithm of [8] corresponds to applying the ADMM algorithm to the dual problem (4.15) that can be formulated as

$$\min_{s \in \tilde{\mathcal{H}}} \left(G^* \circ (-A^*)(s) + F^*(s)\right), \tag{4.23}$$

while retrieving at each iteration the primal iterates in order to solve the primal problem (4.13). The following proposition, which was initially proved in [44], shows that applying the ADMM algorithm to the dual (4.15) is equivalent to solving the primal (4.13) using DR. More precisely, the dual variable (the Lagrange multiplier) $v^{(\ell)}$ of the ADMM iterations is equal to the primal variable $z^{(\ell)}$ of the DR iterations. This result was further extended by [37], which showed the equivalence of ADMM with the proximal point algorithm and proposed several generalizations. For the sake of completeness, we detail the proof of this result using our own notation.

Proposition 4. *Setting*

$$H = G^*, \quad K = F^*, \quad \text{and} \quad B = -A^*, \tag{4.24}$$

the DR iterations (4.7) *with functionals* (4.14) *and* $\alpha = 1$ *are recovered from the ADMM iterations* (4.17) *using*

$$\begin{aligned} v^{(\ell)} &= z^{(\ell)}, \\ \gamma q^{(\ell)} &= w^{(\ell)} - z^{(\ell)}, \\ \gamma A^* s^{(\ell+1)} &= z^{(\ell)} - w^{(\ell+1)}. \end{aligned}$$

Proof. Denoting $\bar{s}^{(\ell)} = A^* s^{(\ell)} \in \mathrm{Im}(A^*)$ (recall that $B = -A^*$ is injective), using the change of notation (4.24), and using the result of Proposition 3, the iterates (4.19) read

$$\begin{aligned} -\bar{s}^{(\ell+1)} &= q^{(\ell)} - u^{(\ell)} + \frac{1}{\gamma}\mathrm{Prox}_{\gamma F \circ A}\left(\gamma(u^{(\ell)} - q^{(\ell)})\right), \\ q^{(\ell+1)} &= u^{(\ell)} - \bar{s}^{(\ell+1)} - \frac{1}{\gamma}\mathrm{Prox}_{\gamma G}\left(\gamma(u^{(\ell)} - \bar{s}^{(\ell+1)})\right), \\ u^{(\ell+1)} &= u^{(\ell)} - \bar{s}^{(\ell+1)} - q^{(\ell+1)}, \end{aligned} \tag{4.25}$$

where we have used the fact that $\operatorname{Prox}_{\gamma F\circ(-A)}(z) = -\operatorname{Prox}_{\gamma F\circ A}(-z)$. Recall that the DR iterations (4.7) read in the setting $\alpha = 1$

$$\begin{aligned} w^{(\ell+1)} &= w^{(\ell)} + \operatorname{Prox}_{\gamma F\circ A}(2z^{(\ell)} - w^{(\ell)}) - z^{(\ell)}, \\ z^{(\ell+1)} &= \operatorname{Prox}_{\gamma G}(w^{(\ell+1)}). \end{aligned} \tag{4.26}$$

Iterations (4.25) and (4.26) are using the following identification between $(q^{(\ell)}, q^{(\ell+1)}, u^{(\ell)}, \bar{s}^{(\ell+1)})$ and $(w^{(\ell)}, z^{(\ell)}, w^{(\ell+1)}, z^{(\ell+1)})$:

$$\gamma(u^{(\ell)} - q^{(\ell)}) = 2z^{(\ell)} - w^{(\ell)}, \tag{4.27}$$

$$\gamma(u^{(\ell)} - \bar{s}^{(\ell+1)}) = w^{(\ell+1)}, \tag{4.28}$$

$$\gamma(u^{(\ell)} - q^{(\ell)} - \bar{s}^{(\ell+1)}) = w^{(\ell+1)} + z^{(\ell)} - w^{(\ell)}, \tag{4.29}$$

$$\gamma(u^{(\ell)} - q^{(\ell+1)} - \bar{s}^{(\ell+1)}) = z^{(\ell+1)}. \tag{4.30}$$

Solving the linear system (4.27)–(4.30), one gets

$$\gamma u^{(\ell)} = z^{(\ell)}, \tag{4.31}$$

$$\gamma q^{(\ell)} = w^{(\ell)} - z^{(\ell)}, \tag{4.32}$$

$$\gamma \bar{s}^{(\ell+1)} = z^{(\ell)} - w^{(\ell+1)}, \tag{4.33}$$

$$\gamma q^{(\ell+1)} = w^{(\ell+1)} - z^{(\ell+1)}. \tag{4.34}$$

First notice that relations (4.32) and (4.34) are compatible at iterations ℓ and $\ell+1$. Then, identifying the update of the variable u presented in (4.25) with relation (4.30), we recover $z^{(\ell+1)} = \gamma u^{(\ell+1)} = v^{(\ell+1)}$, which corresponds to the relation (4.31) at iteration $\ell+1$. ■

This proposition thus shows that, on a centered grid, ALG2 of [8] gives the same iterates as DR on the primal problem. Since we consider a staggered grid, the use of the interpolation operator makes our optimization problem (4.6) different from the original ALG2 and requires the introduction of an auxiliary variable V. Furthermore, the introduction of an extra relaxation parameter α is useful to speed up the convergence of the method, as will be established in the experiments. Finally, let us recall that it is possible to use the variants A-DR', S-DR, and S-DR' of the initial A-DR formulation, as detailed in section 4.4.

5. Generalized cost functions.

Following [35, 20], we propose to use a generalized cost function that allows one to compute geodesics that interpolate between the L^2-Wasserstein and the H^{-1} geodesics. To introduce further flexibility, we introduce spatially varying weights, which corresponds to approximating a transportation problem on a Riemannian manifold.

5.1. Spatially varying interpolation between L^2-Wasserstein and H^{-1}.

We define our discretized generalized transportation problem as

$$\min_{U\in\mathcal{E}_s} \mathcal{J}^w_\beta(\mathcal{I}(U)) + \iota_{\mathcal{C}}(U), \tag{5.1}$$

where the vector of weights $w = (w_k)_{k\in\mathcal{G}_c}$ satisfies $c < w_k \leqslant +\infty$ and $c > 0$ is a small constant. Note that we allow for infinite weights $w_k = +\infty$, which corresponds to forbidding the transport to put mass in a given cell indexed by k. The generalized functional reads, for $\beta \geqslant 0$,

$$\mathcal{J}_\beta^w(V) = \sum_{k \in \mathcal{G}_c} w_k J_\beta(m_k, f_k), \tag{5.2}$$

$$\forall\,(m,f) \in \mathbb{R}^d \times \mathbb{R}, \quad J_\beta(m,f) = \begin{cases} \frac{\|m\|^2}{2f^\beta} & \text{if } f > 0, \\ 0 & \text{if } (m,f) = (0,0), \\ +\infty & \text{otherwise.} \end{cases} \tag{5.3}$$

Note that $\mathcal{J}_1^1 = \mathcal{J}$ and that, for $\beta \in [0,1]$, $\mathcal{J}_\beta^w$ is convex. Furthermore, one has for $f > 0$

$$\det(\partial^2 J_\beta(m,f)) = \frac{\beta(1-\beta)\|m\|^2}{f^{3\beta+2}}. \tag{5.4}$$

This shows that J_β is strictly convex on $\mathbb{R}^{*,d} \times \mathbb{R}^{+,*}$ for $\beta \in]0,1[$.

The case of constant weights $w_k = 1$ is studied in [35, 20]. The case $\beta = 1$ corresponds to the L^2-Wasserstein distance. In a continuous (not discretized) domain, the value of problem (5.1) is equal to the H^{-1} Sobolev norm over densities $\|f_0 - f_1\|_{H^{-1}}$, as detailed in [35]. Note that since in this case the induced distance is actually a Hilbertian norm, the corresponding geodesic is a linear interpolation of the input measures, and thus for measures having densities, one obtains $f_t = (1-t)f_0 + tf_1$.

When $\beta = 1$ and the weights w_k are constant in time, the solution of (5.2) discretizes the displacement interpolation between the densities (f^0, f^1) for a ground cost that is the squared geodesic distance on a Riemannian manifold (see section 1.1 for more details). Note that we restrict our attention to isotropic Riemannian metrics (which are proportional to the identity at each point), but this extends to arbitrary Riemannian or even Finsler metrics. Studying the properties of this transportation distance is, however, not the purpose of this work, and we show in section 6.3 numerical illustrations of the influence of w.

5.2. Computing $\mathrm{Prox}_{\gamma J_\beta}$.

The following proposition, which generalizes Proposition 1, shows how to compute $\mathrm{Prox}_{\gamma \mathcal{J}_\beta^w}$.

Proposition 5. *One has*

$$\forall\, V \in \mathcal{E}_c, \quad \mathrm{Prox}_{\gamma \mathcal{J}_\beta^w}(V) = (\mathrm{Prox}_{\gamma w_k J_\beta}(V_k))_{k \in \mathcal{G}_c},$$

where, for all $(\tilde{m}, \tilde{f}) \in \mathbb{R}^d \times \mathbb{R}$,

$$\mathrm{Prox}_{\gamma J_\beta}(\tilde{m}, \tilde{f}) = \begin{cases} (\mu(f^\star), f^\star) & \text{if } f^\star > 0 \text{ and } \gamma < \infty, \\ (0,0) & \text{otherwise,} \end{cases}$$

$$\text{where} \quad \forall\, f \geqslant 0, \quad \mu(f) = \frac{f^\beta \tilde{m}}{f^\beta + \gamma} \in \mathbb{R}^d \tag{5.5}$$

and $f^\star$ *is the largest real root of the following equation in* X*:*

$$P_\beta(X) = X^{1-\beta}(X - \tilde{f})(X^\beta + \gamma)^2 - \frac{\gamma}{2}\beta\|\tilde{m}\|^2 = 0. \tag{5.6}$$

Proof. We define $(\bar m, \bar f) = \operatorname{Prox}_{\gamma J_\beta}(\tilde m, \tilde f)$, and

$$\forall\,(m,f) \in \mathbb{R}^d \times \mathbb{R}, \quad \Phi_\beta(m,f) = \frac{1}{2}\|(m,f) - (\tilde m, \tilde f)\|^2 + \gamma J_\beta(m,f).$$

If $\bar f > 0$, since Φ_β is C^1 and is strongly convex on $\mathbb{R}^d \times \mathbb{R}^{+,*}$, necessarily $(\bar m, \bar f)$ is the unique solution of $\nabla \Phi_\beta(\bar m, \bar f) = 0$, which reads

$$\begin{cases} \gamma \frac{\bar m}{\bar f^\beta} + \bar m - \tilde m = 0, \\ -\gamma\beta \frac{\|\bar m\|^2}{2\bar f^{\beta+1}} + \bar f - \tilde f = 0. \end{cases}$$

Reformulating these equations leads to the following equivalent conditions:

$$P_\beta(\bar f) = 0 \quad \text{and} \quad \bar m = \mu_\beta(\bar f).$$

This shows that if P_β has at least one strictly positive real root $f^\star$, it is necessarily unique and that $(\bar f = f^\star, \bar m = \mu_\beta(f^\star))$. Otherwise, necessarily $(\bar f = 0, \bar m = 0)$. ■

Note that when $\beta = p/q \in \mathbb{Q}$ is a rational number, $P_\beta(X) = 0$ corresponds to finding the root of a polynomial. It can be solved efficiently using a few Newton descent iterations starting from a large enough value of f.

6. Numerical simulations.

6.1. Comparison of proximal schemes.

This section compares the following algorithms introduced in section 4:

- Douglas–Rachford (DR), as described in section 4.4, parameterized with α and γ;
- ADDM on the dual (ADDM, which is DR with $\alpha = 1$) parameterized with γ;
- Primal-dual (PD), as described in section 4.5, parameterized with σ and τ.

Note that this ADMM formulation is related to the ALG2 method introduced in [8], but is computed over a staggered grid. For the DR algorithm, we first compared the four possible implementations previously described. It appears in our experiments that A-DR and A-DR' (resp., S-DR and S-DR') have almost the same behavior.

The first comparison is done on a simple example with two 2-D isotropic Gaussian distributions (f^0, f^1) with the same variance. In the continuous case, the solution is known to be a translation between the mean of the Gaussians. The spatial domain is here of dimension $d = 2$, and it is discretized on a grid with $N = M = 32$ points for each dimension. The temporal discretization has also been fixed to $P = 32$. We first compute an (almost) exact reference solution $(m^\star, f^\star)$ of the discrete problem with 10^6 iterations of the DR. The obtained transported mass $f^\star(\cdot, t)$ is illustrated in Figure 1. Regarding the computation time, with a biprocessor system Intel Core i7 with 2.4 GHz, 1000 iterations are done in 45 seconds for a 32^3 domain with our MATLAB implementation.

For each algorithm, we perform an exhaustive search of the best possible set of parameters. These optimal parameters are those minimizing $\|(m^\star, f^\star) - (m^{(\ell)}, f^{(\ell)})\|$, the ℓ^2 distance between $f^\star$ and the output of the algorithm after $\ell = 500$ iterations. The optimal parameters for this data set are $\gamma = 1/80$ for ADMM on the dual, $(\gamma = 1/75, \alpha = 1.998)$ for DR, and

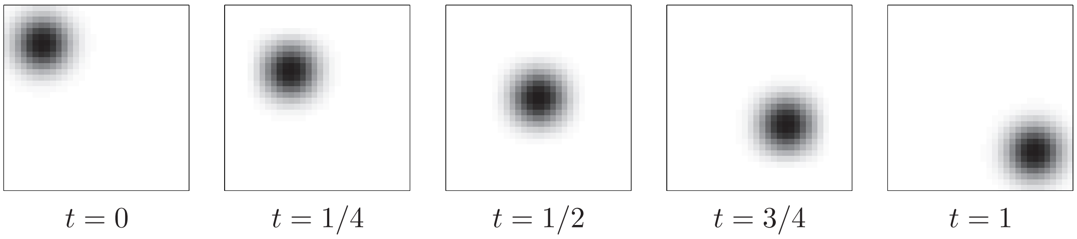

Figure 1. *Display of $f^\star(\cdot, t)$ for several values of t. (Note that for $t = 0$ and $t = 1$ this corresponds to f^0 and f^1.) The grayscale values are linearly interpolating from black to white between 0 and the maximum value of $f^\star$.*

$\sigma = 85$ for PD. For PD, we found that simply setting $\tau = \frac{0.99}{\sigma\|\mathcal{I}\|^2}$ leads to an almost optimal convergence rate in our tests, so we use this rule to only introduce a single parameter σ. Notice that this parameter choice is within the range of parameters $\sigma\tau\|\mathcal{I}\|^2 < 1$ that guarantees convergence of the PD method. Figure 2 displays, for this optimal choice of parameters, the evolution of the cost function value as well as the convergence on the staggered grid toward $(m^\star, f^\star)$ as a function of the iteration number ℓ.

One can observe that the quality of the approximation cannot easily be deduced from the cost function evolution alone since the functional is very flat. Indeed, an almost minimal value of the function is reached by all the algorithms after roughly 10^3 iterations, whereas the ℓ^2 distance to the reference solution continues to decrease almost linearly in log-log scale. The last plot of Figure 2 shows that, asymptotically, all methods tend to satisfy the positivity constraint on the staggered grid at the same rate.

When comparing the three approaches, A-DR and A-PD show the fastest convergence rate to the reference solution, and then the S-DR algorithm performs equally as well as ADMM. This shows the advantage of introducing the α parameter, while symmetrizing the DR does not speed up the convergence. Notice also that the computational cost is smaller for PD, as it takes 0.13s for one PD iteration and 0.2s for one DR or ADMM iteration for this example. Note that these convergence results are related to this specific example, but they illustrate the general behavior of the different algorithms.

Finally, Figure 3 shows an experiment in the context of vanishing and irregular densities. This figure shows the geodesic, computed with the PD algorithm, between two characteristic functions of two connected sets, one being convex. Note that the geodesic is not composed of characteristic functions of sets, which is to be expected. This shows the ability of our methods to cope with vanishing densities.

6.2. Interpolation between L^2-Wasserstein and H^{-1}.

We first apply the PD algorithm for different values of β on the bump example introduced in the previous section. The results are presented in Figure 4, which shows the level-lines of the estimated densities $f^{(\ell)}(\cdot, t)$ for $\ell = 1000$ iterations. It shows the evolution of the solution between a linear interpolation of the densities ($\beta = 0$) and a displacement interpolation with transport ($\beta = 1$).

Figure 5 shows for $\beta = 1/2$ and $\beta = 3/4$ the evolution of the cost function with the iteration index ℓ, together with the convergence of the estimate to the reference solution $(m^\star, f^\star)$ (obtained after 10^5 iterations of the PD algorithm). We can observe that the behavior

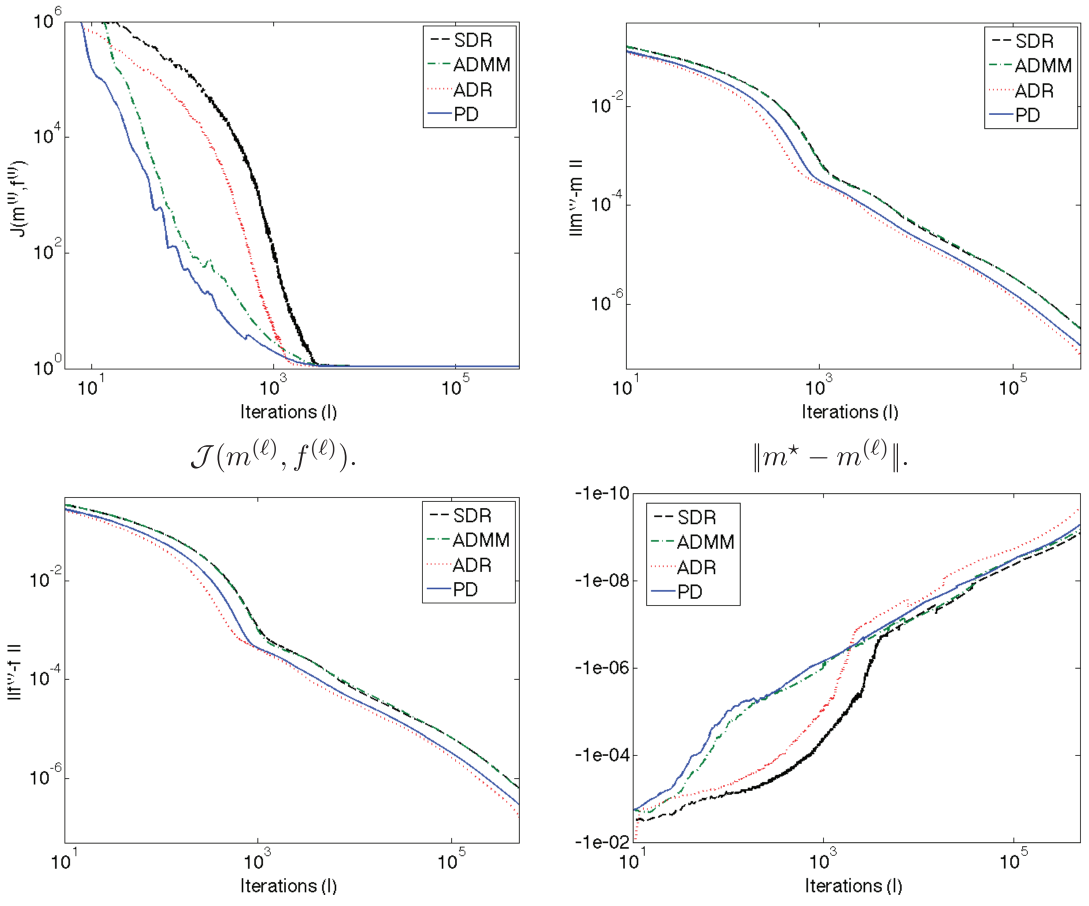

$\mathcal{J}(m^{(\ell)}, f^{(\ell)})$.

$\|m^\star - m^{(\ell)}\|$.

$\|f^\star - f^{(\ell)}\|$.

Minimum value of $f^{(\ell)}$.

Figure 2. *At each iteration ℓ on the staggered grid we plot in log-log scale the value of the cost function $\mathcal{J}$, the distance between the reference solution $(m^\star, f^\star)$ and the estimation $(m^{(\ell)}, f^{(\ell)})$, and the current minimum value of $f^{(\ell)}$ for the different proximal splitting algorithms with the best found parameters.*

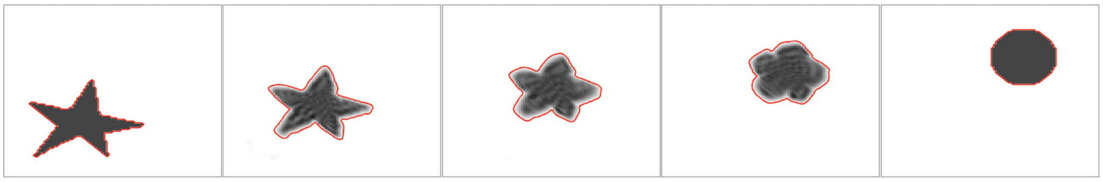

$t = 0$ $t = 1/4$ $t = 1/2$ $t = 3/4$ $t = 1$

Figure 3. *Transport between characteristic functions. Evolution of $f^\star(\cdot, t)$ for several values of t. The red curve denotes the boundary of the area with positive density.*

of the process with $\beta \in]0, 1[$ is different than that observed for $\beta = 1$ in Figure 2. Indeed, we observe a faster convergence of the functional value, which is consistent with the fact that $\mathcal{J}_\beta$ becomes more and more strongly convex as β approaches $1/2$ (see (5.4)). The oscillations come from the Newton's descent that only approximate the computation of $\text{Prox}_{\gamma J_\beta}$.

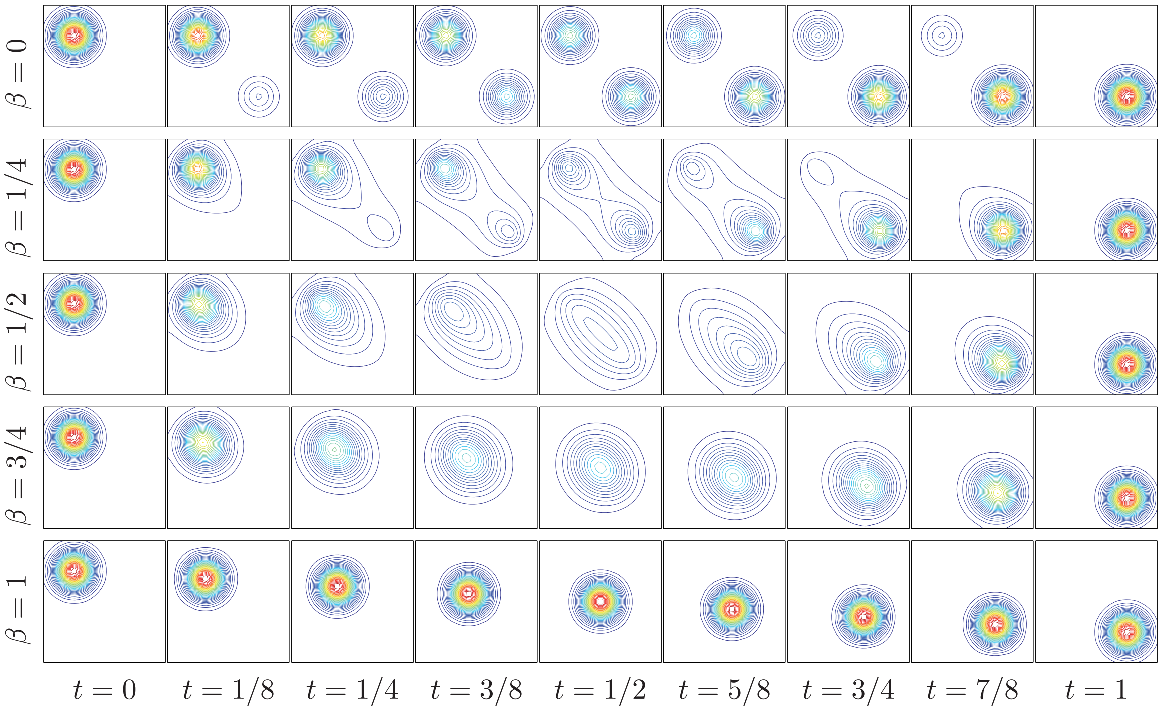

Figure 4. *Display of the level sets of $f^{(\ell)}(\cdot, t)$ for several value of t and β. (Note that for $t = 0$ and $t = 1$, this corresponds to f^0 and f^1.)*

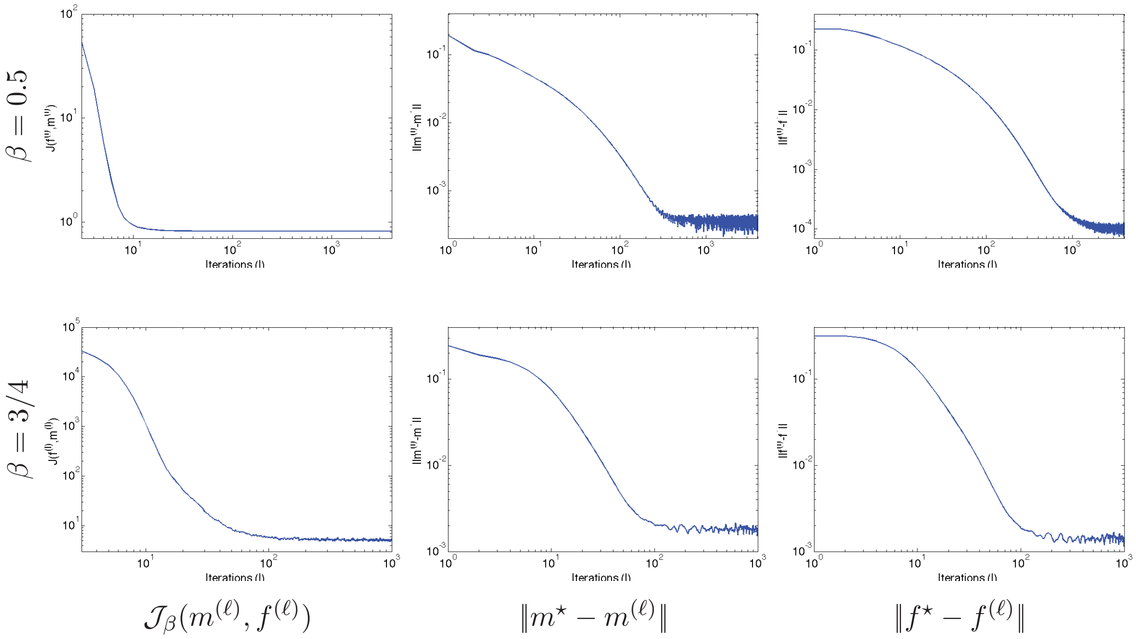

Figure 5. *At each iteration ℓ, we plot the value of the cost function $\mathcal{J}_\beta(m^{(\ell)}, f^{(\ell)})$ and the distance between the reference solution $(m^\star, f^\star)$ and the estimation $(m^{(\ell)}, f^{(\ell)})$. The first (resp., second) row presents the result with $\beta = 1/2$ (resp., $\beta = 3/4$).*

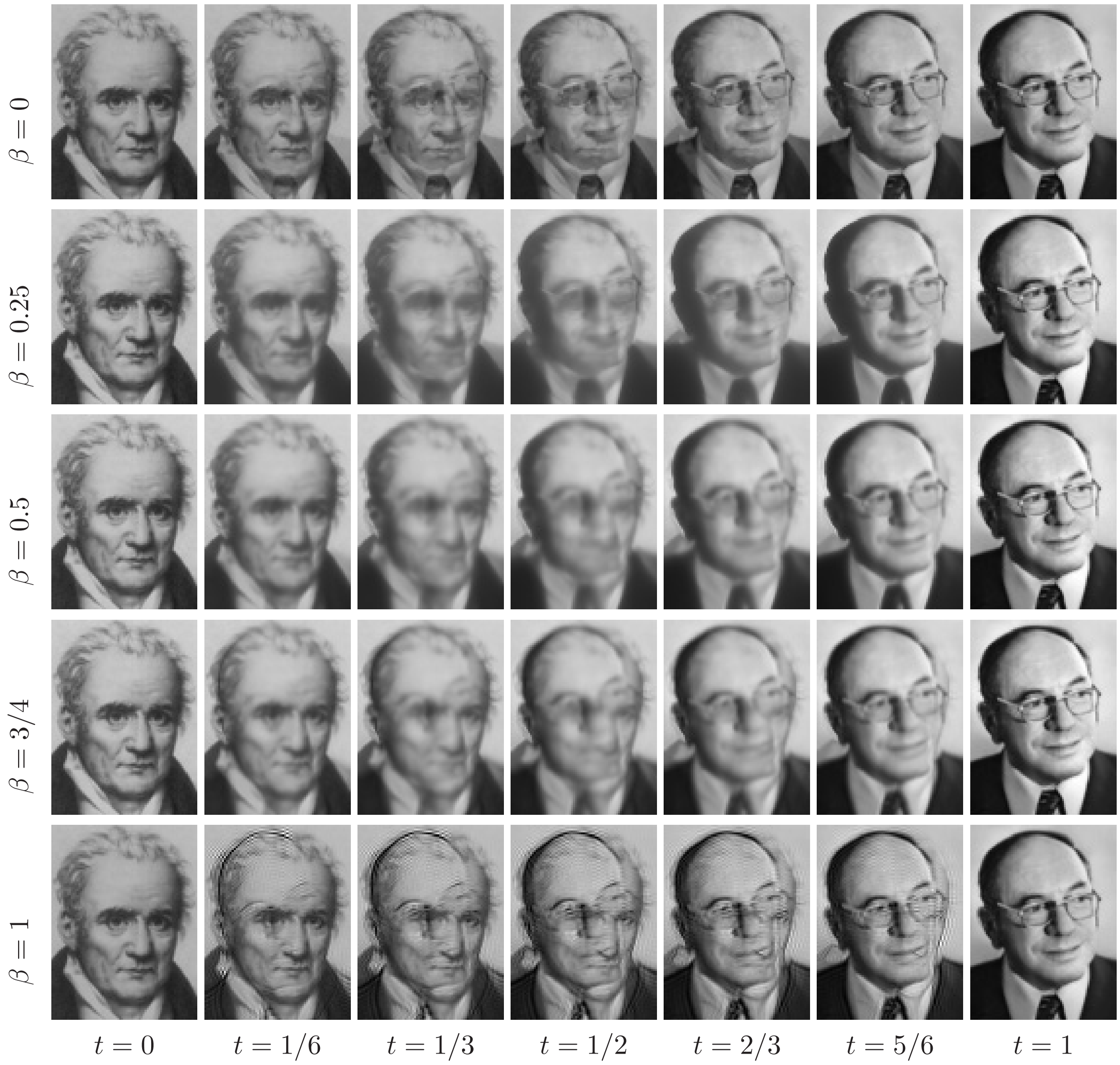

Figure 6. *Evolution of $f^\star(\cdot, t)$ for several value of t and β. The first and last columns represent the data f^0 and f^1. The intermediate ones present the reference solution $f^\star(t)$ for successive times $t = i/6$, $i = 1, \ldots, 5$. Each line illustrates $f^\star$ for different values $\beta = j/4$, $j = 0, \ldots, 4$ of the generalized cost function.*

As a second example, we show in Figure 6 the different morphings obtained between pictures of Gaspard Monge and Leonid Kantorovich. The grayscale representation scales linearly between black (value of 0) and white (value of 1), and the dimensions are $N+1 = 75$, $M+1 = 100$, $P+1 = 60$, M being the number of discrete points in the second spatial dimension.

6.3. Riemannian transportation. We investigate in this section the approximation of a displacement interpolation for a ground cost being the squared geodesic distance on a Riemannian manifold. This is achieved by solving (5.1) with $\beta = 1$ but a nonconstant weight

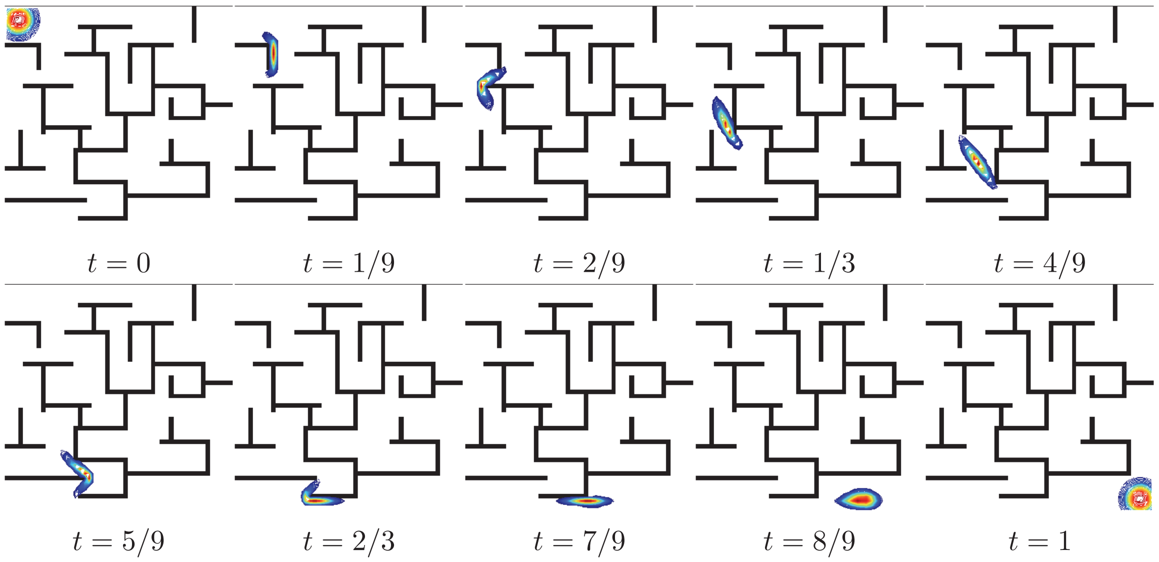
$t = 0$ $t = 1/9$ $t = 2/9$ $t = 1/3$ $t = 4/9$

$t = 5/9$ $t = 2/3$ $t = 7/9$ $t = 8/9$ $t = 1$

Figure 7. *Evolution of $f^\star(\cdot, t)$ for several values of t, using a Riemannian manifold with weights w_k (constant in time) restricting the densities to lie within a 2-D static labyrinth map.*

map w.

We exemplify this setting by considering optimal transport with obstacles, which corresponds to choosing weights w that are infinite on the obstacle $\mathcal{O} \subset \mathbb{R}^d \times \mathbb{R}$; i.e.,

$$\forall\, k \in \mathcal{G}_c, \quad w_k = 1 + \iota_{\mathcal{O}}(x_k, t_k) \in \{1, +\infty\}.$$

Note that the obstacles can be dynamic; i.e., the weight w need not be constant in time.

Figure 7 shows a first example, where $\mathcal{O}$ is a 2-D ($d = 2$) static labyrinth map (the walls of the labyrinth are the obstacles and are displayed in black). We use a $50 \times 50 \times 100$ discretization grid of the space-time domain $[0, 1]^3$, and the input measures (f^0, f^1) are Gaussians with standard deviations equal to 0.04. For Gaussians with such a small variance, this example shows that the displacement interpolation is located close to the geodesic path between the centers of the Gaussians.

Figure 8 shows a more complicated setting that includes a labyrinth with moving walls: a wall appears at time $t = 1/4$, and another one disappears at time $1/2$. The difference with respect to the previous example is the fact that w is now time-dependent. This simple modification has a strong impact on the displacement interpolation. Indeed, the speed of propagation of the mean of the density is not constant anymore since the density measure is confined in a small area surrounded by walls for $t \in [1/4, 1/2]$.

As a last example, we present in Figure 9 an interpolation result in the context of oceanography in the presence of coast. We here consider Gaussian mixture data in order to simulate the sea surface temperature that can be observed from a satellite. In order to model the influence of the sea ground height, we here considered weights w varying w.r.t. the distance to the coast. Denoting as $\mathcal{O}$ the area representing the complementary of the sea, we define

$$\forall\, k \in \mathcal{G}_c, \quad w_k = 1 + d(x_k, \partial\mathcal{O}) + \iota_{\mathcal{O}} \in \{1, +\infty\},$$

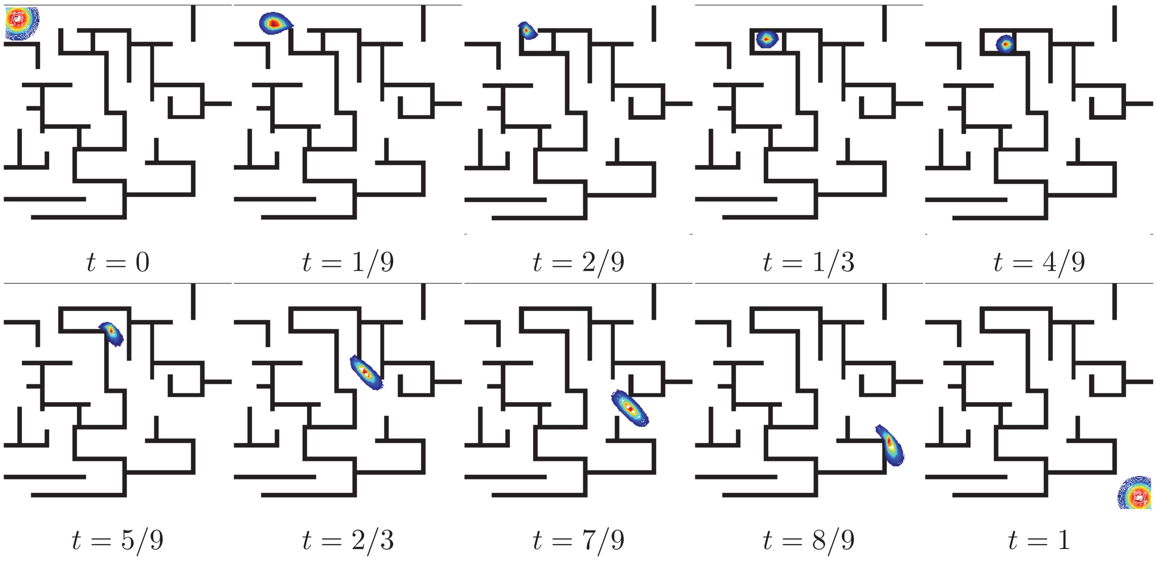

Figure 8. *Evolution of $f^\star(\cdot, t)$ for several values of t, using a Riemannian manifold with weights w_k (evolving in time) restricting the densities to lie within a 2-D dynamic labyrinth map (i.e., with moving walls).*

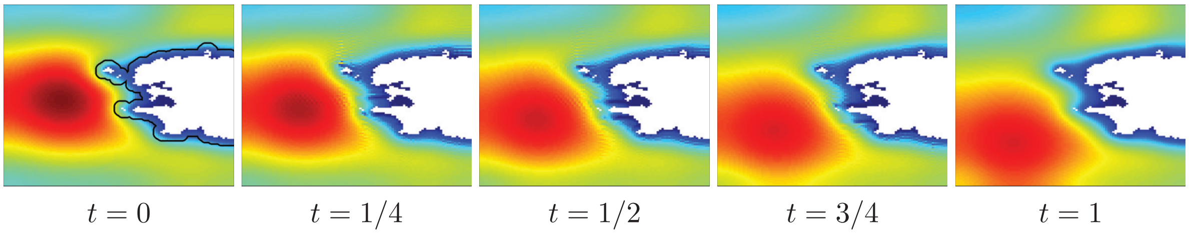

Figure 9. *Evolution of $f^\star(\cdot, t)$ for several values of t, using a Riemannian manifold with weights w_k defined using the distance to the boundary of the sea domain (its frontier is displayed in black in the first figure).*

where $d(x, \partial\mathcal{O})$ is the Euclidean distance between a pixel location x and the boundary of $\mathcal{O}$. The estimation of such interpolations is of main interest in geophysic forecasting applications where the variables of numerical models are calibrated using external image observations (such as the sea surface temperature). Data assimilation methods used in geophysics look for the best compromise between a model and the observations (see, for instance, [12]), and making use of optimal transportation methods in this context is an open research problem.

Conclusion. In this article, we have shown how proximal splitting schemes offer an elegant and unifying framework for describing computational methods for solving dynamical optimal transport with an Eulerian discretization. This allowed us to extend the original method of Benamou and Brenier in several directions, most notably by the use of staggered grid discretization and the introduction of generalized, spatially variant, cost functions.

Acknowledgment. We would like to thank to Jalal Fadili for his detailed explanations of the connection between the ADMM and DR algorithms.

REFERENCES

[1] M. Agueh and G. Carlier, *Barycenters in the Wasserstein space*, SIAM J. Math. Anal., 43 (2011), pp. 904–924.

[2] J. Anderson, *Computational Fluid Dynamics*, McGraw–Hill Science/Engineering/Math, New York, 1995.

[3] S. Angenent, S. Haker, and A. Tannenbaum, *Minimizing flows for the Monge–Kantorovich problem*, SIAM J. Math. Anal., 35 (2003), pp. 61–97.

[4] K. J. Arrow, L. Hurwicz, and H. Uzawa, *Studies in Linear and Non-linear Programming*, Stanford University Press, Stanford, CA, 1958.

[5] J. Benamou and Y. Brenier, *Weak existence for the semigeostrophic equations formulated as a coupled Monge–Ampère/transport problem*, SIAM J. Appl. Math., 58 (1998), pp. 1450–1461.

[6] J.-D. Benamou, *A domain decomposition method for the polar factorization of vector-valued mappings*, SIAM J. Numer. Anal., 32 (1995), pp. 1808–1838.

[7] J.-D. Benamou, *Numerical resolution of an "unbalanced" mass transport problem*, ESAIM Math. Model. Numer. Anal., 37 (2010), pp. 851–868.

[8] J.-D. Benamou and Y. Brenier, *A computational fluid mechanics solution of the Monge-Kantorovich mass transfer problem*, Numer. Math., 84 (2000), pp. 375–393.

[9] J.-D. Benamou and Y. Brenier, *Wasserstein optimal mapping between prescribed densities functions*, J. Optim. Theory Appl., 111 (2001), pp. 255–271.

[10] J.-D. Benamou, B. D. Froese, and A. M. Oberman, *A viscosity solution approach to the Monge–Ampere formulation of the optimal transportation problem*, arXiv:1208.4873, 2013.

[11] D. P. Bertsekas, *The auction algorithm: A distributed relaxation method for the assignment problem*, Ann. Oper. Res., 14 (1988), pp. 105–123.

[12] J. Blum, F.-X. Le Dimet, and I. M. Navon, *Data assimilation for geophysical fluids*, in Handbook of Numerical Analysis 14, Elsevier, New York, 2009, pp. 385–441.

[13] N. Bonneel, M. van de Panne, S. Paris, and W. Heidrich, *Displacement interpolation using Lagrangian mass transport*, ACM Trans. Graphics (Proceedings of SIGGRAPH Asia 2011), 30 (2011), 158.

[14] F. Bornemann and C. Rasch, *Finite-element discretization of static Hamilton-Jacobi equations based on a local variational principle*, Comput. Visual. Sci., 9 (2006), pp. 57–69.

[15] S. Boyd, B. Parikh, E. Chu, B. Peleato, and J. Eckstein, *Distributed optimization and statistical learning via the alternating direction method of multipliers*, Found. Trends Machine Learning, 3 (2011), pp. 1–122.

[16] Y. Brenier, *Polar factorization and monotone rearrangement of vector-valued functions*, Comm. Pure Appl. Math., 44 (1991), pp. 375–417.

[17] L. M. Briceño-Arias and P. L. Combettes, *A monotone+skew splitting model for composite monotone inclusions in duality*, SIAM J. Optim., 21 (2011), pp. 1230–1250.

[18] M. Burger, M. Franek, and C.-B. Schönlieb, *Regularized regression and density estimation based on optimal transport*, Appl. Math. Res. Express. AMRX, (2011).

[19] R. Burkard, M. Dell'Amico, and S. Martello, *Assignment Problems*, SIAM, Philadelphia, 2009.

[20] P. Cardaliaguet, G. Carlier, and B. Nazaret, *Geodesics for a class of distances in the space of probability measures*, Calc. Var. Partial Differential Equations, (2012), pp. 1–26.

[21] J. A. Carrillo and J. S. Moll, *Numerical simulation of diffusive and aggregation phenomena in nonlinear continuity equations by evolving diffeomorphisms*, SIAM J. Sci. Comput., 31 (2009), pp. 4305–4329.

[22] A. Chambolle and T. Pock, *A first-order primal-dual algorithm for convex problems with applications to imaging*, J. Math. Imaging Vision, 40 (2011), pp. 120–145.

[23] P. Clarysse, B. Delhay, M. Picq, and J. Pousin, *Optimal extended optical flow subject to a statistical constraint*, J. Comput. Appl. Math., 234 (2010), pp. 1291–1302.

[24] P. L. Combettes and J.-C. Pesquet, *A Douglas-Rachford splitting approach to nonsmooth convex variational signal recovery*, IEEE J. Selected Topics Signal Process., 1 (2007), pp. 564–574.

[25] P. L. Combettes and J.-C. Pesquet, *Proximal splitting methods in signal processing*, in Fixed-Point Algorithms for Inverse Problems in Science and Engineering, Springer, New York, 2011, pp. 185–212.

[26] P. L. Combettes and J.-C. Pesquet, *A proximal decomposition method for solving convex variational inverse problems*, Inverse Problems, 24 (2011), 065014.

[27] D. Cordero-Erausquin, B. Nazaret, and C. Villani, *A mass-transportation approach to sharp Sobolev and Gagliardo-Nirenberg inequalities*, Adv. Math., 182 (2004), pp. 307–332.

[28] G. B. Dantzig, *Linear Programming and Extensions*, Princeton University Press, Princeton, NJ, 1963.

[29] F. de Goes, D. Cohen-Steiner, P. Alliez, and M. Desbrun, *An optimal transport approach to robust reconstruction and simplification of 2D shapes*, Computer Graphics Forum, 30 (2011), pp. 1593–1602.

[30] E. J. Dean and R. Glowinski, *An augmented Lagrangian approach to the numerical solution of the Dirichlet problem for the elliptic Monge-Ampère equation in two dimensions*, Electron. Trans. Numer. Anal., 22 (2006), pp. 71–96.

[31] J. Delon, *Movie and video scale-time equalization application to flicker reduction*, IEEE Trans. Image Process., 15 (2006), pp. 241–248.

[32] J. Delon, J. Salomon, and A. Sobolevski, *Fast transport optimization for Monge costs on the circle*, SIAM J. Appl. Math., 70 (2010), pp. 2239–2258.

[33] J. Delon, J. Salomon, and A. Sobolevskii, *Local matching indicators for transport problems with concave costs*, SIAM J. Discrete Math., 26 (2012), pp. 801–827.

[34] J. Digne, D. Cohen-Steiner, P. Alliez, F. Goes, and M. Desbrun, *Feature-preserving surface reconstruction and simplification from defect-laden point sets*, J. Math. Imaging Vision, (2013), pp. 1–14.

[35] J. Dolbeault, B. Nazaret, and G. Savaré, *A new class of transport distances between measures*, Calc. Var. Partial Differential Equations, 34 (2009), pp. 193–231.

[36] B. During, D. Matthes, and J. P. Milisic, *A gradient flow scheme for nonlinear fourth order equations*, Discrete Contin. Dyn. Syst. Ser. B, 14 (2010), pp. 935–959.

[37] J. Eckstein and D. P. Bertsekas, *On the Douglas-Rachford splitting method and the proximal point algorithm for maximal monotone operators*, Math. Programming, 55 (1992), pp. 293–318.

[38] X. Feng and M. Neilan, *Mixed finite element methods for the fully nonlinear Monge–Ampère equation based on the vanishing moment method*, SIAM J. Numer. Anal., 47 (2009), pp. 1226–1250.

[39] S. Ferradans, G.-S. Xia, G. Peyré, and J.-F. Aujol, *Static and dynamic texture mixing using optimal transport*, in Proceedings of the Fourth International Conference on Scale Space and Variational Methods in Computer Vision (SSVM'13), Lecture Notes in Comput. Sci. 7893, Springer, Berlin, Heidelberg, 2013, pp. 137–148.

[40] L. Ferragut and I. Asensio, *Mixed finite element methods for a class of nonlinear reaction diffusion problems*, Neural Parallel Sci. Comput., 10 (2002), pp. 91–112.

[41] M. Fortin and R. Glowinski, *Augmented Lagrangian Methods: Applications to the Numerical Solution of Boundary-Value Problems*, Elsevier Science, New York, 1983.

[42] U. Frisch, S. Matarrese, R. Mohayaee, and A. Sobolevski, *A reconstruction of the initial conditions of the universe by optimal mass transportation*, Nature, 417 (2002), pp. 260–262.

[43] B. D. Froese, *A numerical method for the elliptic Monge–Ampère equation with transport boundary conditions*, SIAM J. Sci. Comput., 34 (2012), pp. A1432–A1459.

[44] D. Gabay, *Applications of the method of multipliers to variational inequalities*, in Augmented Lagrangian Methods: Applications to the Solution of Boundary Value Problems, M. Fortin and R. Glowinski, eds., North–Holland, Amsterdam, 1983, pp. 299–340.

[45] D. Gabay and B. Mercier, *A dual algorithm for the solution of nonlinear variational problems via finite element approximation*, Comput. Math. Appl., 2 (1976), pp. 17–40.

[46] R. Glowinski and A. Marroco, *Sur l'approximation, par éléments finis d'ordre un, et la résolution, par pénalisation-dualité d'une classe de problèmes de Dirichlet non linéaires*, ESAIM Math. Model. Numer. Anal. Modél. Math. Anal. Numér., 9 (1975), pp. 41–76.

[47] H. W. Kuhn, *The Hungarian method of solving the assignment problem*, Naval Res. Logistics Quart., 2 (1955), pp. 83–97.

[48] E. Haber, T. Rehman, and A. Tannenbaum, *An efficient numerical method for the solution of the L_2 optimal mass transfer problem*, SIAM J. Sci. Comput., 32 (2010), pp. 197–211.

[49] S. Haker, L. Zhu, A. Tannenbaum, and S. Angenent, *Optimal mass transport for registration and warping*, Int. J. Computer Vision, 60 (2004), pp. 225–240.

[50] F. H. Harlow and J. E. Welch, *Numerical calculation of time-dependent viscous incompressible flow of fluid with free surface*, Phys. Fluids, 8 (1965), pp. 2182–2189.

[51] A. Iollo and D. Lombardi, *A Lagrangian scheme for the solution of the optimal mass transfer problem*, J. Comput. Phys., 230 (2011), pp. 3430–3442.

[52] R. Jordan, D. Kinderlehrer, and F. Otto, *The variational formulation of the Fokker–Planck equation*, SIAM J. Math. Anal., 29 (1998), pp. 1–17.

[53] Y.-H. Kim and B. Pass, *Multi-marginal Optimal Transport on Riemannian Manifolds*, preprint, arXiv: 1303.6251, 2013.

[54] R. Kimmel and J. A. Sethian, *Computing geodesic paths on manifolds*, Proc. Natl. Acad. Sci., 95 (1998), pp. 8431–8435.

[55] H. Ling and K. Okada, *An efficient earth mover's distance algorithm for robust histogram comparison*, IEEE Trans. Pattern Anal. Machine Intell., 29 (2007), pp. 840–853.

[56] P. L. Lions and B. Mercier, *Splitting algorithms for the sum of two nonlinear operators*, SIAM J. Numer. Anal., 16 (1979), pp. 964–979.

[57] R. J. McCann, *Polar factorization of maps on Riemannian manifolds*, Geom. Funct. Anal., 11 (2001), pp. 589–608.

[58] R. J. McCann, *A convexity principle for interacting gases*, Adv. Math., 128 (1997), pp. 153–179.

[59] Q. Mérigot, *A multiscale approach to optimal transport*, Computer Graphics Forum, 30 (2011), pp. 1583–1592.

[60] J. J. Moreau, *Proximité et dualité dans un espace hilbertien*, Bull. Soc. Math. France, 93 (1965), pp. 273–299.

[61] Y. Nesterov and A. Nemirovskii, *Interior Point Polynomial Methods in Convex Programming*, Stud. Appl. Math. 13, SIAM, Philadelphia, 1994.

[62] A. M. Oberman, *Wide stencil finite difference schemes for the elliptic Monge-Ampere equation and functions of the eigenvalues of the Hessian*, Discrete Contin. Dyn. Syst. Ser. B, 1 (2008), pp. 221–238.

[63] V. I. Oliker and L. D. Prussner, *On the numerical solution of the equation* $\frac{\partial^2 z}{\partial x^2}\frac{\partial^2 z}{\partial y^2} - (\frac{\partial^2 z}{\partial x \partial y})^2 = f$ *and its discretizations*, Numer. Math., 3 (1988), pp. 271–293.

[64] N. Papadakis, E. Provenzi, and V. Caselles, *A variational model for histogram transfer of color images*, IEEE Trans. Image Process., 20 (2011), pp. 1682–1695.

[65] O. Pele and M. Werman, *Fast and robust earth mover's distances*, in Proceedings of the IEEE International Conference on Computer Vision (ICCV'09), 2009, pp. 460–467.

[66] N. Pustelnik, C. Chaux, and J. Pesquet, *Parallel proximal algorithm for image restoration using hybrid regularization*, IEEE Trans. Image Process., 20 (2011), pp. 2450–2462.

[67] J. Rabin and G. Peyré, *Wasserstein regularization of imaging problem*, in Proceedings of the IEEE International Conference on Image Processing (ICIP'11), 2011, pp. 1541–1544.

[68] J. Rabin, G. Peyré, J. Delon, and M. Bernot, *Wasserstein barycenter and its application to texture mixing*, in Proceedings of the Conference Scale Space and Variational Methods in Computer Vision (SSVM'11), Lecture Notes in Comput. Sci. 6667, Springer, Berlin, 2011, pp. 435–446.

[69] Y. Rubner, C. Tomasi, and L. J. Guibas, *A metric for distributions with applications to image databases*, in Proceedings of the IEEE International Conference on Computer Vision (ICCV'98), 1998, pp. 59–66.

[70] J. A. Sethian, *A fast marching level set method for monotonically advancing fronts*, Proc. Natl. Acad. Sci. USA, 93 (1996), pp. 1591–1595.

[71] S. Shirdhonkar and D. W. Jacobs, *Approximate earth mover's distance in linear time*, in Proceedings of the IEEE Conference on Computer Vision and Pattern Recognition (CVPR'08), 2008, pp. 1–8.

[72] J. E. Spingarn, *Applications of the method of partial inverses to convex programming: Decomposition*, Math. Programming, 32 (1985), pp. 199–223.

[73] G. Strang, *Linear Algebra and Its Applications*, Brooks Cole, Pacific Grove, CA, 1988.

[74] M. Sulman, J. F. Williams, and R. D. Russell, *Optimal mass transport for higher dimensional adaptive grid generation*, J. Comput. Phys., 230 (2011), pp. 3302–3330.

[75] J. Tsitsiklis, *Efficient algorithms for globally optimal trajectories*, IEEE Trans. Automat. Control, 40 (1995), pp. 1528–1538.

[76] C. Villani, *Topics in Optimal Transportation*, Grad. Stud. Math., American Mathematical Society, Providence, RI, 2003.

[77] C. Villani, *Optimal Transport: Old and New*, Grundl. Math. Wiss. 338, Springer, Berlin, 2009.